

Pacific hotspots reveal a Louisville–Ontong Java Nui tectonic link

<https://doi.org/10.1038/s41586-025-08889-0>

Received: 21 September 2021

Accepted: 7 March 2025

Published online: 30 April 2025

 Check for updates

J. G. Konter^{1,8}, V. A. Finlayson^{1,2✉}, K. Konrad³, M. G. Jackson⁴, A. A. P. Koppers³, P. Wessel^{1,8}, S. Beethé³, M. Bizimis⁵, A. Alverson⁶ & C. Kelley⁷

Volcanic hotspots are thought to form by melting in an upwelling mantle plume head followed by melting of the plume tail. Plate motion then generates an age-progressive volcanic track originating from a large igneous province to a currently active hotspot. The most voluminous large igneous province, the approximately 120-million-year-old Ontong Java Nui Plateau (OJP-Nui) in the mid-Pacific, however, lacks an obvious volcanic track. Although the Louisville hotspot track was originally proposed as a candidate, limited constraints for Pacific absolute plate and plume motion before 80 million years ago (Ma) suggest a mismatch¹. Existing Pacific models rely on age–distance data from the continuous Hawai‘i–Emperor and Louisville tracks, but their tracks older than approximately 80 Ma are subducted. Elsewhere on the Pacific Plate, only discontinuous seamount tracks that formed before 80 Ma are documented^{2–7}. Currently, models require approximately 1,200 kilometres of latitudinal motion to link the Louisville plume to the OJP-Nui¹, but palaeolatitude estimates from about 70 Ma to today remain within error of its present location^{8,9}, suggesting that any substantial Louisville plume motion occurred earlier. Here, through a combination of geochemistry and geochronology^{9–14}, we demonstrate that Samoa and Rurutu–Arago are the longest-lived Pacific hotspots, traceable to more than 100 Ma before subducting into the Mariana Trench. These tracks better constrain plate rotation between 80 Ma and 100 Ma, allowing us to update Pacific absolute plate motion models and link the Louisville volcanic track to OJP-Nui without requiring major plume motion.

Plume-fed hotspots show age-progressive volcanic tracks that often originate from a large igneous province (LIP), which marks a hotspot’s inception^{15–18}. Eruption of a LIP is thought to correspond to the arrival of the head of a deeply rooted mantle plume, causing extensive melting in the upper mantle and unusually voluminous eruptions comprising the LIP^{3,19,20}. The Ontong-Java Plateau (OJP; Fig. 1) once formed the greater Ontong-Java Nui Plateau (OJP-Nui), together with the Manihiki and Hikurangi plateaus²¹. Despite a proposed plume origin^{22,23}, there is no obvious age-progressive volcanic track emerging from the plateau. Although the Louisville hotspot was proposed to be related²⁴, later palaeomagnetic data failed to definitively link the Louisville hotspot to the OJP^{22,25–28}, whereas geochemical evidence supported a link between Louisville and parts of the Manihiki Plateau²⁹. Recently obtained Louisville palaeomagnetic latitudes are constant within error up to about 70 million years ago (Ma)⁸, suggesting that any Louisville plume motion should precede 70 Ma. In that time frame, existing absolute plate motion (APM) models require about 1,200 km of plume motion to place Louisville and the OJP in the same original eruptive location¹. However, more recent geochemical data revealing similar neodymium

(Nd)–lead (Pb)–strontium (Sr) systematics between the main phase of the OJP-Nui system and the Louisville seamount track are permissive of the Louisville–OJP connection^{29,30} (Fig. 2). Despite increasing evidence for a direct geochemical Louisville–OJP connection, the lack of support for such a link through existing tectonic reconstructions has persisted until this study. Here we show that the two longest-lived Pacific hotspot tracks—Samoa and Rurutu–Arago^{9,14} (see below)—yield an APM model that supports a genetic link between the Louisville hotspot track and the OJP-Nui, the largest LIP preserved in the geologic record.

Most existing Pacific APM models rely significantly on the Hawai‘i–Emperor and Louisville hotspots back to 80 Ma, whereas unrelated discontinuous volcanic structures are used for Pacific Plate motion before 80 Ma (refs. 2,3,7,18,31,32; Fig. 1 and Extended Data Fig. 1). These structures include the Shatsky Rise, Hess Rise, Mid-Pacific Mountains, Line Islands, Lili‘uokalani Seamounts, Musicians Seamounts, Wake Seamounts, Marshall Islands and Magellan Seamounts. From these, the Mid-Pacific Mountains and Shatsky Rise erupted near all-ridge triple junctions, whereas Hess Rise and Musicians Seamounts erupted near-ridge^{31–34} (Extended Data Fig. 2). Plume–ridge interactions could

¹Department of Earth Sciences, School of Ocean and Earth Science and Technology, University of Hawai‘i at Mānoa, Honolulu, HI, USA. ²Department of Geology, University of Maryland, College Park, MD, USA. ³College of Earth, Ocean and Atmospheric Sciences, Oregon State University, Corvallis, OR, USA. ⁴Department of Earth Science, University of California Santa Barbara, Santa Barbara, CA, USA. ⁵School of the Earth, Ocean, and Environment, University of South Carolina, Columbia, SC, USA. ⁶Department of Earth, Environmental and Planetary Sciences, Brown University, Providence, RI, USA. ⁷Department of Oceanography, School of Ocean and Earth Science and Technology, University of Hawai‘i at Mānoa, Honolulu, HI, USA. ⁸Deceased: J. G. Konter, P. Wessel. ✉e-mail: vfinlays@umd.edu

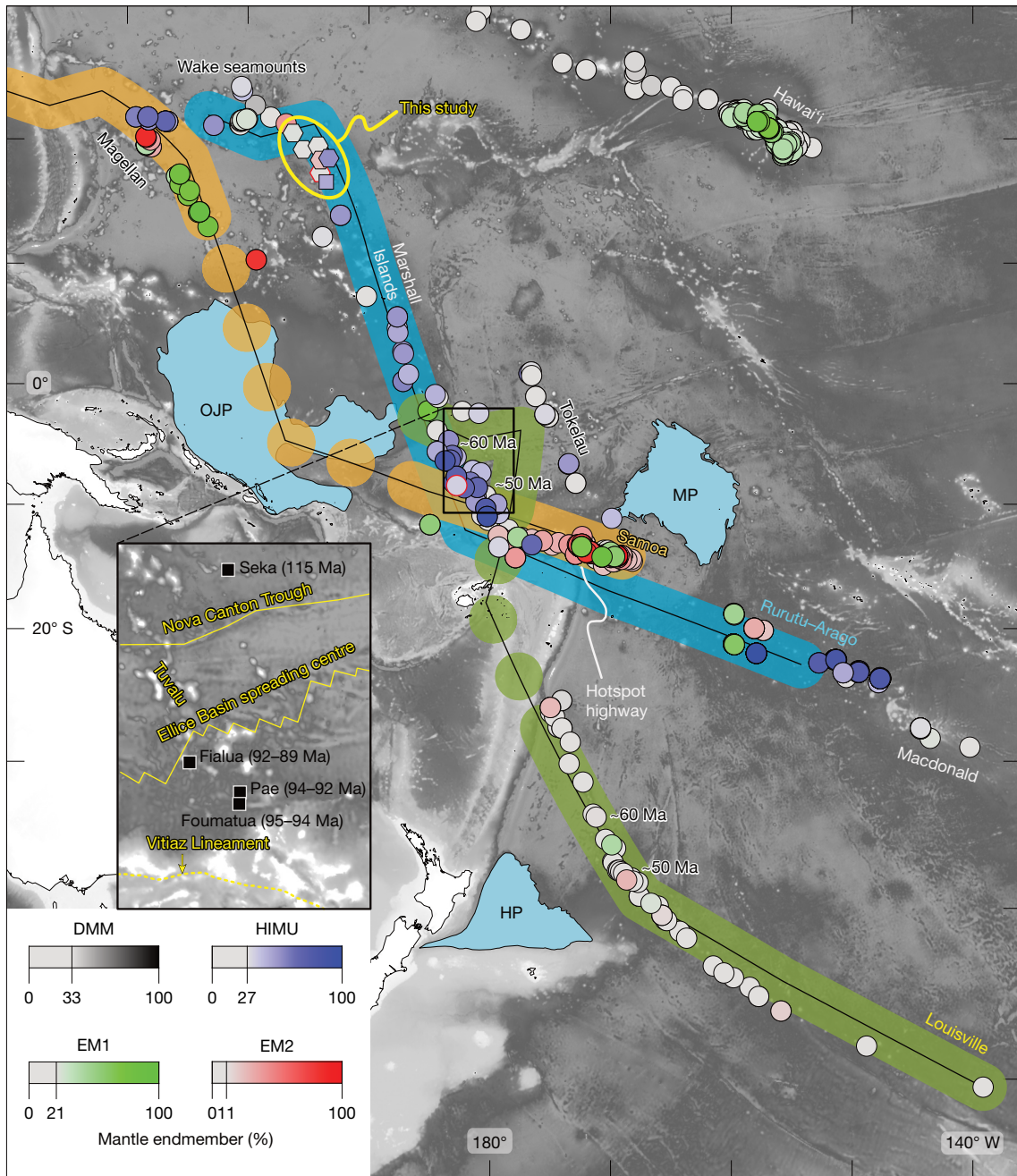


Fig. 1 | Map of Pacific hotspot tracks and geochemical lava flow compositions. Sample data^{9,14,29,31,46,56–65} for Pacific hotspot tracks show unique signatures for Rurutu–Arago (blue-to-grey circles; see Methods for details on colour-coding) and Samoa (red and green) and thus allow for the effective geochemical tracing of these hotspots, when combined with seamount ages. The Wake Island region samples linked to Rurutu–Arago are shown as hexagons; a Wake sample unrelated to Rurutu–Arago (Methods) is shown with a square symbol. The Ellice Basin group and Wake samples with a red outline are confirmed as phosphatized (see ‘Alteration’ section in Methods) and not considered in discussions of ¹⁴³Nd/¹⁴⁴Nd behaviour. The coloured tracks show predicted hotspot tracks following the K01m APM (specifically, 80–100-Ma stage represented by the Wake–Marshall and Magellan areas). The dashed portions of the predicted

Louisville hotspot track mark where the track was subducted. For Louisville (green), the updated APM predicts an origin at the OJP. The APM modelling relies on Wake–Marshall and Magellan seamounts, omitting the Shatsky and Mid-Pac groups, and directly relates the Louisville hotspot to the OJP. Hawaiian–Emperor hotspot sample data are shown for reference. See Supplementary Tables 1–3 for the isotopic, compositional, data and age determinations presented in this study. Inset: locations and ages of all Ellice Basin seamounts and Seka Seamount, as confirmed by geochronology, as black squares. The Tuvalu chain, Nova Canton Trough, Ellice Basin spreading centre and Vitiāz Lineament are shown in yellow. MP, Manihiki Plateau; HP, Hikurangi Plateau; DMM, depleted MORB (mid-ocean ridge basalt) mantle; EM1, enriched mantle 1; EM2, enriched mantle 2; HIMU high μ ($\mu = ^{238}\text{U}/^{204}\text{Pb}$).

significantly displace the upwelling mantle plume³⁵ such that resulting (unresolved) plume motion is inadvertently included in APM models. Moreover, the Line Islands lack a clear age progression³⁶, the Musicians Seamounts are complicated by overprinting of deformation-related volcanism³⁵, and Shatsky Rise was recently suggested to be controlled

by seafloor spreading³⁷. In summary, all these structures are unlikely to exclusively represent APM, yet only the Wake, Marshall and Magellan seamounts appear to be truly intraplate before 80 Ma (Extended Data Fig. 2). As we propose, they represent the Cretaceous portions of two long-lived Pacific hotspots—Samoa and Rurutu–Arago—that can

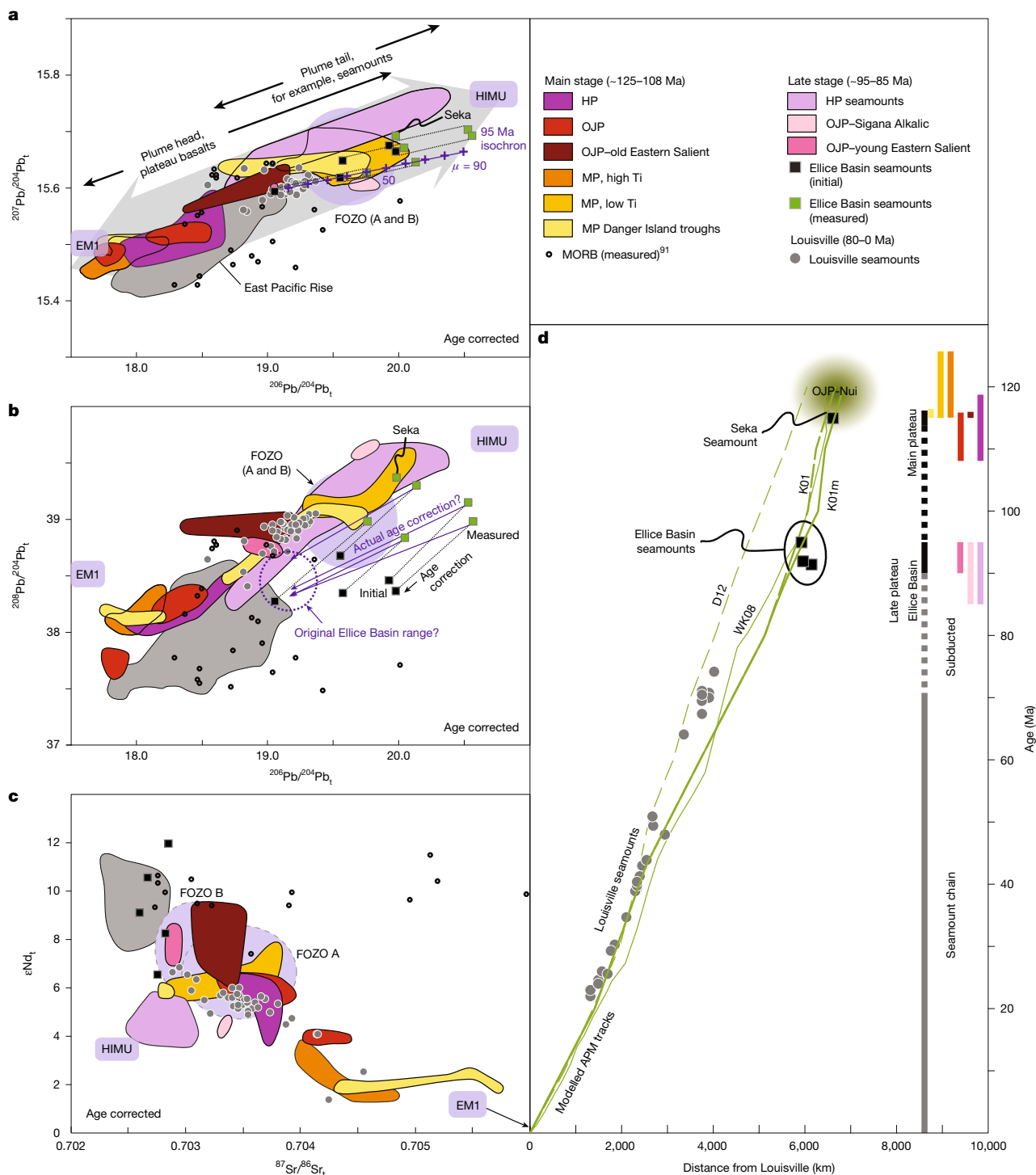


Fig. 2 | Geochemistry and geochronology of volcanic structures linked to the OJP-Nui and Louisville system. **a**, Age-corrected (denoted by the subscript *t*) $^{207}\text{Pb}/^{204}\text{Pb}$ versus $^{206}\text{Pb}/^{204}\text{Pb}$ isotope compositions for OJP-Nui, and related structures. **b**, Age-corrected $^{208}\text{Pb}/^{204}\text{Pb}$ versus $^{206}\text{Pb}/^{204}\text{Pb}$ isotope compositions for OJP-Nui, and related structures. **c**, $e^{143}\text{Nd}$ versus age-corrected $^{87}\text{Sr}/^{86}\text{Sr}$ for OJP-Nui and related structures. **d**, Age progression for the Louisville hotspot track (symbols same as in plots). Ellice Basin seamounts¹⁴ and Seka Seamount⁴⁶ are shown. Pb isotope data for OJP, MP and HP, which represent the main pulses of voluminous plateau-building volcanism (about 120 Ma and about 90 Ma)^{23,25,30,66–72}, are frequently less radiogenic, but extend to radiogenic values in some settings. By contrast, smaller structures such as seamounts are confined to intermediate-to-radiogenic values. Louisville and Ellice Basin seamounts show more radiogenic Pb (**a**, **b**) and Nd (**c**) isotopes, with some Ellice Basin samples being particularly radiogenic owing to varying degrees of seawater uranium

influence and phosphatization, respectively¹⁴. Despite alteration resulting in superficial resemblance to HIMU-like Danger Island (**b**) or DMM-like (**c**) compositions, the Ellice Basin seamounts sampled a mixture of FOZO⁷³ and DMM⁷⁴ (Supplementary Information) that may have originally resembled slightly depleted Louisville-type^{29,30} compositions. Green squares are present-day Ellice Basin compositions, compared with corresponding age-corrected (where possible) compositions. Louisville seamount data overlap directly with some OJP basalts in the Pb–Nd–Sr isotope space^{29,30}, and are well within the array of compositions found in the greater combined set of plateaus and structures from the OJP, MP and HP. Furthermore, Ellice Basin and Seka seamounts are spatiotemporally linked to the OJP. See Methods for a description of the isotopic data compared with variations in plume head and plume tail stages of volcanic activity and analysis of Pb–Sr–Nd isotopic systematics in the Ellice Basin samples. Panels **a–c** adapted with permission from ref. 69, Elsevier.

extend Hawai'i–Emperor and Louisville anchored Pacific APM models to the 80–120-Ma period.

The clearly defined Hawai'i–Emperor and Louisville hotspot tracks provide a continuous hotspot record for APM modelling back to approximately 80 Ma, where they subduct into the Kamchatka and Tonga trenches, respectively^{8,38} (Fig. 1 and Extended Data Fig. 1). However, changing palaeomagnetic latitudes³⁹, predictions of hotspot motion based on Indo-Atlantic hotspots⁴⁰, and inter-hotspot differences in age progressions and distances^{9,41,42} all suggest relative motion between these two plumes and the Pacific Plate. Supporting this contention, models using global mantle flow to predict plume motions have been argued to provide a better fit to the actual hotspot tracks across ocean basins than fixed plume models⁶. The improved fit incorporating these geodynamic models suggests that some hotspot tracks provide a combined record of plate motion and plume motion^{3,5,18}, although fixed-hotspot models reproduce most tracks to first order.

On the Pacific Plate, the Rurutu–Arago volcanic track—defined from young to old by the Cook–Austral islands, the Tuvalu islands, the Marshall Islands and Wake seamounts—represents a third long-lived hotspot in addition to Hawai'i–Emperor and Louisville (Fig. 1). Changes in the distance between these three hotspots from 60 Ma to 50 Ma suggest that the Hawai'i–Emperor hotspot moved more significantly and mostly independently from both Louisville and Rurutu–Arago⁹. However, more critical here is the fact that the Rurutu–Arago and Samoan hotspots can be traced further back into the Cretaceous period than Hawai'i and Louisville. The older portions of the Rurutu–Arago and Samoa hotspots both extend into the West Pacific, where tracing their tracks through the high density of Cretaceous seamounts has required the mapping out of well-defined age progressions combined with distinctive geochemical signatures^{4,12,14} (Fig. 1 and Extended Data Figs. 3 and 4).

To this end, we present isotope geochemistry and, where possible, age determinations from seamounts around Wake Island, a critical geological nexus that links the older (>80 Ma) segment of the long-lived Rurutu–Arago hotspot track to the younger (<80 Ma) portion originating in the Cook–Austral islands^{4,12,14,43,44}. We use this hotspot track, together with the long-lived Samoan hotspot track, to generate an APM stage pole between 80 Ma and 100 Ma that resolves the apparent disconnect between the OJP–Nui and the Louisville hotspot.

Tracing long-lived hotspot tracks

The extreme and distinct hotspot compositions originating in the central Pacific⁴³ have generated clearly traceable hotspot tracks (Fig. 1 and Extended Data Fig. 4). We reveal these tracks using colour-coding (Fig. 1) based on the $^{87}\text{Sr}/^{86}\text{Sr}$ – $^{143}\text{Nd}/^{144}\text{Nd}$ – $^{206}\text{Pb}/^{204}\text{Pb}$ isotopic compositions of lavas at each volcano along the hotspot tracks^{9–14,45,46}. In particular, elevated $^{206}\text{Pb}/^{204}\text{Pb}$ compositions are an identifying feature of the Rurutu–Arago hotspot and can be traced back into the western Pacific along an age progression (blue-to-grey symbols in Fig. 1; Extended Data Fig. 4). However, north of the Marshall Islands, a data gap in the Rurutu–Arago hotspot track separated these ≤ 80 -Ma volcanoes from the ≥ 100 -Ma Wake seamounts, complicating efforts to trace the Rurutu–Arago track before 80 Ma. Our recent sampling of seamounts around Wake Island fills this gap and Pb–Sr–Nd isotopic compositions (Methods) of these samples match those of the rest of the Rurutu–Arago hotspot track (Extended Data Figs. 4 and 5). We also present an age of 91.3 Ma from a Wake Island seamount (Extended Data Table 1, Supplementary Table 3 and Methods) that places it directly on the Rurutu–Arago hotspot age progression (Extended Data Fig. 4).

Farther west, the Cretaceous Magellan seamounts also span the approximately 80–100-Ma age range⁴ and overlap with the Samoan hotspot in composition. Critically, the age and location of these seamounts matches the predicted track of Samoa (Fig. 1 and Extended Data Fig. 4) that, until now, could be traced only from the present-day

location near the northern terminus of the Tonga Trench to about 25-Ma Alexa Bank⁴⁷, west of which the trace of the Samoan hotspot is lost in the Vitiaz Trench. The predicted Samoan hotspot track passes through the OJP, where its large lithospheric thickness²⁰ probably suppressed Samoan plume melting and volcanic construction⁴⁸. The predicted hotspot therefore is expected to emerge on the north side of the OJP as 80–100-Ma volcanoes, which is consistent with the age and location of the Magellan seamounts. Further supporting a link to the Samoan hotspot, the Magellan seamounts feature the same unique combination of intermediate $^{206}\text{Pb}/^{204}\text{Pb}$ and extreme radiogenic $^{87}\text{Sr}/^{86}\text{Sr}$ isotope compositions observed in Samoan shield lavas¹⁰ (Fig. 1, red), and are capped by late-stage volcanism with a characteristic low $^{206}\text{Pb}/^{204}\text{Pb}$ and elevated $^{87}\text{Sr}/^{86}\text{Sr}$ isotope composition^{46,49} (Fig. 1, green, and Extended Data Fig. 6). Magellan seamount compositions and ages⁴ are reassessed here, revealing a Samoan shield to rejuvenated stage isotopic sequence⁴⁹ at Hemler and Vlinder seamounts, whereas samples obtained from the younger Magellan seamounts are similar to Samoan late-stage rejuvenated compositions (Extended Data Fig. 6).

New constraints on old plate motion

APM models for the predicted tracks of the high $^{206}\text{Pb}/^{204}\text{Pb}$ Rurutu–Arago hotspot and the high $^{87}\text{Sr}/^{86}\text{Sr}$ Samoa hotspot suggest that these two hotspot tracks should continue into the Mariana Trench^{7,50} (Fig. 1). Geochemical data on Mariana arc volcanoes provide further support that the Rurutu–Arago and Samoa hotspot tracks are subducted near the region proposed by APM models. When the isotopic compositions of the Mariana arc volcanoes are examined, an unusual geographically constrained high $^{206}\text{Pb}/^{204}\text{Pb}$ anomaly^{48–51} and an adjacent high $^{87}\text{Sr}/^{86}\text{Sr}$ anomaly (which overlaps, but is shifted slightly to the south) are found where the Rurutu–Arago and Samoa hotspot tracks are predicted to subduct based on the revised APM model (Fig. 1 and Extended Data Fig. 7). Consistent with the hypothesis that the subduction of seamounts impacts the chemistry of nearby arc volcanoes, the $^{206}\text{Pb}/^{204}\text{Pb}$ and $^{87}\text{Sr}/^{86}\text{Sr}$ anomalies in the Mariana arc^{51,52} provide supporting evidence for the presence of the long-lived Rurutu–Arago and Samoan hotspot tracks in the western Pacific during the Early Cretaceous. Furthermore, their offset position in the Mariana arc also supports the presence of a more northerly Rurutu–Arago hotspot track in the western Pacific region predicted by our APM, which is different from predictions by previous APM models (Fig. 1 and Extended Data Fig. 7). Consequently, we now can explore Rurutu–Arago and Samoa as a pair of long-lived parallel (but offset) hotspot tracks, providing a multi-hotspot continuation of APM constraints beyond the 80-Ma limit that is provided by the Hawai'i–Emperor and Louisville hotspot tracks.

Although the Rurutu–Arago hotspot track is defined by seamounts with related geochemical fingerprints that closely follow APM models back to 80 Ma, existing APM models⁷ predict its track to significantly bend around Wake Island (Extended Data Fig. 7) and extend thousands of kilometres westwards below the South and North Wake seamount trails (Fig. 1). This region is only sparsely populated by seamounts when compared with the abundance of seamounts around Wake Island itself (extending north from the Marshall Islands) and the east–west-oriented Wake seamount trails, which together provide a clear morphological continuation of the hotspot track. Previously published geochemical and temporal data^{31,50} and our data on seven seamounts around Wake Island suggest a match to the Rurutu–Arago hotspot (Extended Data Fig. 7) in the 80–100-Ma time frame. The clear impact of the Rurutu–Arago hotspot track on Mariana arc compositions^{50,51} (Extended Data Fig. 7) suggests that, in contrast to existing APM models, the hotspot track followed a more northerly track between 120 Ma and 80 Ma—resulting in an offset of >1,200 km from existing models. This alternative 'northern path' (blue path in the Wake seamounts in Fig. 1, and 'this study' in Extended Data Fig. 7) for Rurutu–Arago provides a unified

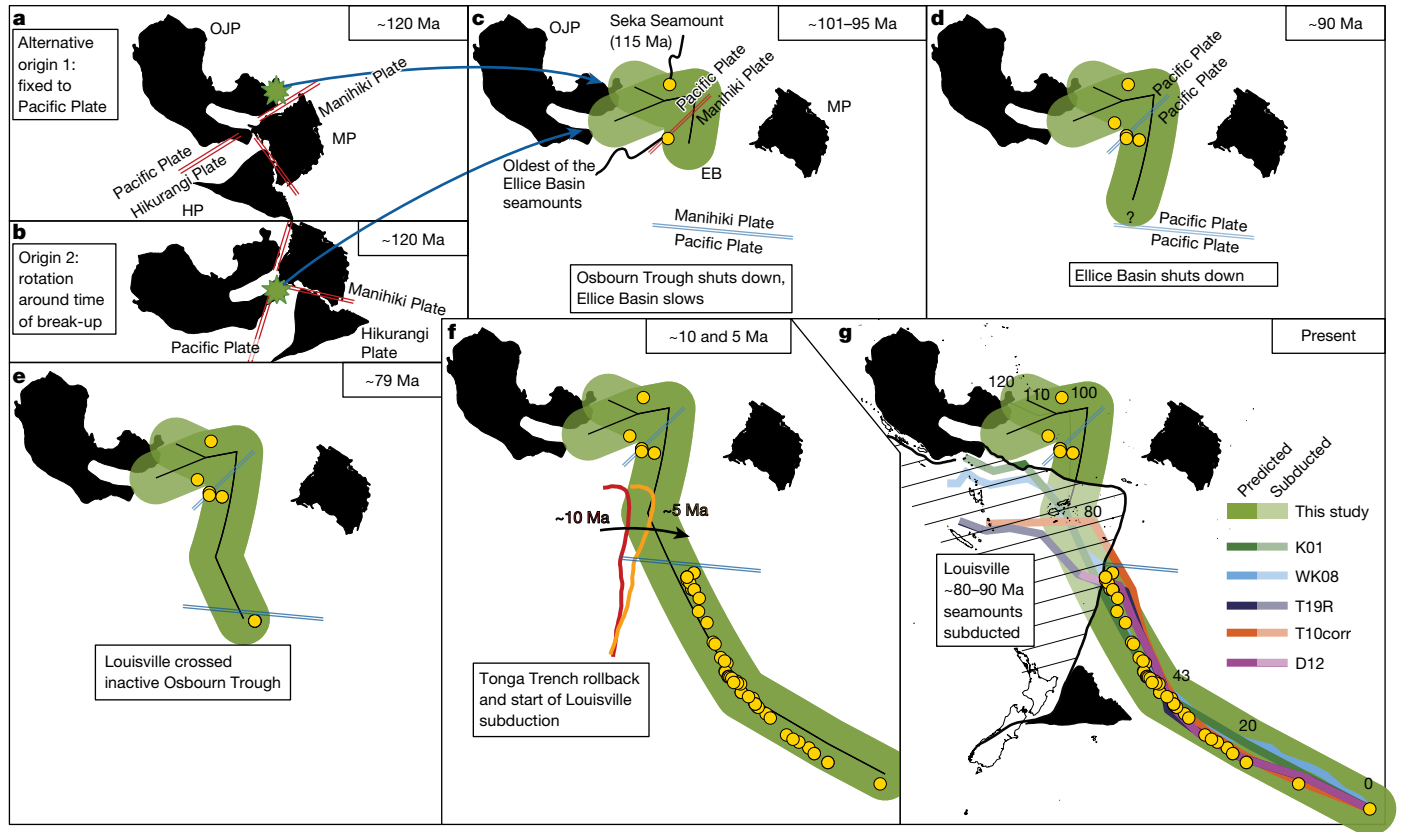


Fig. 3 | Cartoon of Louisville hotspot evolution. **a, b**, The revised model predicts that the Louisville hotspot (green swath) initiated within the OJP; however, the exact initial location is sensitive to whether the plateaus rotated around the time of OJP-Nui break-up⁵⁴, so two alternatives are shown for approximately 120 Ma: origin 1 (**a**) and origin 2 (**b**). **c**, By approximately 95 Ma, the Ellice Basin (EB) had (mostly) opened between the OJP and the MP, as suggested by the age of the oldest Ellice Basin seamounts (95.0 Ma (ref. 14))—located centrally in the basin—which we link to the Louisville hotspot. Seka Seamount (115.0 Ma (ref. 46)), located at the north end of the basin, is isotopically similar to the Ellice Basin seamounts (suggesting that significant Ellice Basin spreading occurred by 115 Ma) and is also linked to the Louisville hotspot. **d**, Our model predicts Louisville to be present in the Ellice Basin at this time,

progressing to younger ages to the south by 90 Ma. **e**, The oldest Louisville seamount that erupted at about 79 Ma (refs. 8, 38), located south of the Osborn Trough, represents the oldest part of the continuously defined Louisville hotspot track. **f, g**, In the past 5 Ma to 10 Ma (**f**), roll-back of the Tonga Trench caused the subduction⁷⁵ of any Louisville seamounts with ages between 79 Ma and 90 Ma, leaving only the older (>90 Ma) Louisville hotspot-related structures in the Ellice Basin and OJP areas preserved to the present day (**g**). Consequently, the relationship between >79-Ma Louisville hotspot volcanism and the palaeoridge represented by the Osborn Trough is unclear. Predicted hotspot tracks^{6,18,41,53,76} show that only our model tracks the Louisville hotspot back to the OJP-Nui, specifically the OJP. See Methods for details on this model.

explanation for all these observations—geochronological, geochemical and geomorphological—suggesting that a reconsideration of the Pacific Plate APM model is warranted. The period of plate motion covered by our data is constrained by the approximately 80–100-Ma Marshall Island volcanoes and Wake Island area seamounts. Critically, new and existing ⁴⁰Ar/³⁹Ar ages for the two volcanic chains correspond to the 80–100-Ma single-plate rotation (stage) of the existing K01 plate motion model¹⁸. For the period before 80 Ma, modern APM models⁵³ still define motion with the large time-step plate rotations of early models^{2,18}. Given the limited availability of samples suitable for age determinations around Wake Island, we resort to a similar approach as used in the K01 model³ and calculate plate motion using large time-steps rather than applying a more continuous age model such as WK08⁴¹. For the 80–100-Ma time interval, we modelled the plate motion by finding a singular stage pole (0.7° S, 315.7° E) that minimizes the difference in Euler pole distance between the actual seamounts and the predicted age-progressive paths for the Samoa and Rurutu–Arago hotspot tracks (Methods and Extended Data Fig. 8). Using the modified APM model, called K01m, our results show that the predicted track projects Rurutu–Arago through the Wake-area seamounts (blue path in Fig. 1), whereas previous models failed to reconstruct the positions of the >100-Ma Wake Islands and

seamounts (Extended Data Fig. 7). Owing to the southeasterly shift in location of the K01m rotation pole compared with K01, the relative angular distances from the Euler pole to Samoa and Rurutu—have changed in a manner where the resulting predicted path length for Samoa remains similar to older models, whereas that of Rurutu–Arago lengthens significantly.

The OJP-Nui–Louisville connection

The application of this 80–100-Ma rotation pole to the Louisville hotspot has profound implications for linking the Louisville track to the OJP-Nui. Whereas previous plate motion models placed the Louisville hotspot far from the OJP at the time of eruption¹, the 80–100-Ma rotation increases the north–south component of the predicted Louisville path (Fig. 3). As a result, the K01m model using long-lived intraplate hotspots traces the predicted Louisville hotspot track directly into the centre of OJP-Nui by about 120 Ma, the modelled age of formation for the superplateau^{21,54}. This is in contrast to existing APM models^{3,6,7,53}, which all predict a more southerly track (Fig. 3) that falls short of the OJP-Nui, most likely because these models incorporate near-ridge large structures (rises) and seamounts in their datasets. An assessment of the fit of individual track segments using backtracking with different

APM models confirms this result (Methods and Extended Data Fig. 9). The formation age of the OJP has been estimated based on decades-old lower-quality $^{40}\text{Ar}/^{39}\text{Ar}$ ages as well as previous plate reconstructions to be older than 120 Ma (refs. 21,54); however, recent high-precision geochronology suggests that the main phase of OJP volcanism began around 116 Ma (ref. 55). This makes the reconstructed link between Louisville and OJP-Nui even more likely.

During the formation of the Louisville hotspot track from the OJP-Nui until the present day (Fig. 3), there remains two time periods with poor constraints. First, the 80–90-Ma Louisville seamounts all have subducted into the Tonga Trench, interrupting the direct connection between the OJP and the Louisville seamount track. Second, the location of the earliest portion of the Louisville seamount track between 90 Ma and 116 Ma depends on whether or not the Manihiki or Hikurangi plates (and their associated plateaus) rotated during the break-up¹ of the OJP-Nui (Fig. 3), and whether there exists an eruptive age progression throughout the OJP-Nui given that Manihiki may pre-date the OJP by up to 6 Ma (ref. 55). In either case, the eruptive location of the earliest Louisville track is within the OJP-Nui outline and, importantly, we show that 90–115-Ma seamounts in the Ellice Basin agree with the expected age progression, location and isotopic signature of Louisville hotspot-related volcanoes in the region¹⁴ (Fig. 2). These seamounts therefore provide the ‘missing link’ connecting the OJP to the start of the Louisville track. The Louisville seamount and Ellice Basin seamount data, despite evidence of secondary alteration in the latter, are geochemically similar and plot along the array defined by Manihiki’s Danger Islands and OJP melts (Fig. 2, Extended Data Fig. 10 and Supplementary Information). Therefore, the Louisville and Ellice Basin seamounts are geochemically and temporally linked to the OJP-Nui.

Our demonstrated fit of the OJP-Nui to the Louisville hotspot track (Fig. 3 and Extended Data Fig. 8) requires no significant plume motion, which agrees with estimates of limited latitudinal motion of this hotspot between about 70 Ma and 0 Ma (ref. 8). Our 80–100-Ma data from the Wake Island region, and our interpretation of existing data from the Rurutu–Arago, Samoa and OJP-Nui–Louisville hotspot systems, thus present a simple argument for the genetic connection between Louisville and the OJP-Nui. This implies a plume-driven origin for the largest LIP in the geologic record, in contrast to recent arguments for a major role for seafloor spreading in the construction of LIPs, such as Shatsky Rise³⁶. Renewed consideration for other Cretaceous ‘orphan’ LIPs—that may still lack obvious volcanic trails—is warranted, in light of the suggested revision to the 80–100-Ma stage pole that may serve to further address identified uncertainties in Pacific APM during the Cretaceous.

Online content

Any methods, additional references, Nature Portfolio reporting summaries, source data, extended data, supplementary information, acknowledgements, peer review information; details of author contributions and competing interests; and statements of data and code availability are available at <https://doi.org/10.1038/s41586-025-08889-0>.

- Chandler, M. T., Wessel, P. & Sager, W. W. Analysis of Ontong Java Plateau palaeolatitudes: evidence for large-scale rotation since 123 Ma? *Geophys. J. Int.* **194**, 18–29 (2013).
- Duncan, R. A. & Clague, D. A. in *The Ocean Basins and Margins: Volume 7A The Pacific Ocean* (eds Nairn, A. E. M. et al.) 89–121 (Springer, 1985).
- Koppers, A. A. P. et al. Mantle plumes and their role in Earth processes. *Nat. Rev. Earth Environ.* **2**, 382–401 (2021).
- Koppers, A. A. P. & Sager, W. W. in *Developments in Marine Geology* Vol. 7 (eds Stein, R. et al.) 553–597 (Elsevier, 2014).
- Tarduno, J. A., Bunge, H.-P., Sleep, N. & Hansen, U. The bent Hawaiian–Emperor hotspot track: inheriting the mantle wind. *Science* **324**, 50–53 (2009).
- Dobrovine, P. V., Steinberger, B. & Torsvik, T. H. Absolute plate motions in a reference frame defined by moving hot spots in the Pacific, Atlantic, and Indian oceans. *J. Geophys. Res. Solid Earth* **117**, B09101 (2012).
- Wessel, P. & Kroenke, L. W. Observations of geometry and ages constrain relative motion of Hawaii and Louisville plumes. *Earth Planet. Sci. Lett.* **284**, 467–472 (2009).
- Koppers, A. A. P., Staudigel, H., Phipps Morgan, J. & Duncan, R. A. Nonlinear $^{40}\text{Ar}/^{39}\text{Ar}$ age systematics along the Gilbert Ridge and Tokelau Seamount Trail and the timing of the Hawaii–Emperor bend. *Geochem. Geophys. Geosyst.* **8**, Q06L13 (2007).
- Konrad, K. et al. On the relative motions of long-lived Pacific mantle plumes. *Nat. Commun.* **9**, 854 (2018).
- Jackson, M. G. et al. Helium and lead isotopes reveal the geochemical geometry of the Samoan plume. *Nature* **514**, 355–358 (2014).
- Jackson, M. G. et al. Samoan hot spot track on a “hot spot highway”: implications for mantle plumes and a deep Samoan mantle source. *Geochem. Geophys. Geosyst.* **11**, Q12009 (2010).
- Konter, J. G. & Jackson, M. G. Large volumes of rejuvenated volcanism in Samoa: evidence supporting a tectonic influence on late-stage volcanism. *Geochem. Geophys. Geosyst.* **13**, Q0AM04 (2012).
- Koppers, A. A. P. et al. Limited latitudinal mantle plume motion for the Louisville hotspot. *Nat. Geosci.* **5**, 911–917 (2012).
- Finlayson, V. A. et al. Sr–Pb–Nd–Hf isotopes and $^{40}\text{Ar}/^{39}\text{Ar}$ ages reveal a Hawaii–Emperor-style bend in the Rurutu hotspot. *Earth Planet. Sci. Lett.* **500**, 168–179 (2018).
- Richards, M. A., Duncan, R. A. & Courtillot, V. E. Flood basalts and hot-spot tracks: plume heads and tails. *Science* **246**, 103–107 (1989).
- Courtillot, V., Davaille, A., Besse, J. & Stock, J. Three distinct types of hotspots in the Earth’s mantle. *Earth Planet. Sci. Lett.* **205**, 295–308 (2003).
- Konter, J. G. & Becker, T. W. Shallow lithospheric contribution to mantle plumes revealed by integrating seismic and geochemical data. *Geochem. Geophys. Geosyst.* **13**, Q02004 (2012).
- Koppers, A. A. P., Phipps Morgan, J., Morgan, J. W. & Staudigel, H. Testing the fixed hotspot hypothesis using $^{40}\text{Ar}/^{39}\text{Ar}$ age progressions along seamount trails. *Earth Planet. Sci. Lett.* **16**, 237–252 (2001).
- Campbell, I. H., Griffiths, R. W. & Hill, R. I. Melting in an Archaean mantle plume: heads it’s basalts, tails it’s komatiites. *Nature* **339**, 697–699 (1989).
- Coffin, M. F. & Eldholm, O. Large igneous provinces: crustal structure, dimensions, and external consequences. *Rev. Geophys.* **32**, 1–36 (1994).
- Taylor, B. The single largest oceanic plateau: Ontong Java–Manihiki–Hikurangi. *Earth Planet. Sci. Lett.* **241**, 372–380 (2006).
- Mahoney, J. J. & Spencer, K. J. Isotopic evidence for the origin of the Manihiki and Ontong Java oceanic plateaus. *Earth Planet. Sci. Lett.* **104**, 196–210 (1991).
- Golowin, R. et al. Geochemistry of deep Manihiki Plateau crust: implications for compositional diversity of large igneous provinces in the Western Pacific and their genetic link. *Chem. Geol.* **493**, 553–566 (2018).
- Henderson, L. & Gordon, R. G. Oceanic plateaus and the motion of the Pacific Plate with respect to the hotspots. *EOS Trans. Am. Geophys. Union* **62**, 1028 (1981).
- Mahoney, J. J., Storey, M., Duncan, R. A., Spencer, K. J. & Pringle, M. Geochemistry and age of the Ontong Java Plateau. *Am. Geophys. Union Geophys. Monogr. Ser.* **77**, 233–261 (1993).
- Antretter, M., Riisager, P., Hall, S., Zhao, X. & Steinberger, B. Modelled palaeolatitudes for the Louisville hot spot and the Ontong Java Plateau. *Geol. Soc. Lond. Spec. Publ.* **229**, 21–30 (2004).
- Kroenke, L. W., Wessel, P. & Sterling, A. Motion of the Ontong Java Plateau in the hot-spot frame of reference: 122 Ma–present. *Geol. Soc. Lond. Spec. Publ.* **229**, 9–20 (2004).
- Neal, C., Mahoney, J., Kroenke, L., Duncan, R. & Petterson, M. in *Large Igneous Provinces: Continental, Oceanic, and Planetary Flood Volcanism* (eds Mahoney, J. J. & Coffin, M. F.) 183–216 (American Geophysical Union, 1997).
- Vanderkluyen, L. et al. Louisville seamount chain: petrogenetic processes and geochemical evolution of the mantle source. *Geochem. Geophys. Geosyst.* **15**, 2380–2400 (2014).
- Tejada, M. L. G. et al. New evidence for the Ontong Java Nui hypothesis. *Sci. Rep.* **13**, 8486 (2023).
- Koppers, A. A. P., Staudigel, H., Pringle, M. S. & Wijbrans, J. R. Short-lived and discontinuous intraplate volcanism in the South Pacific: hot spots or extensional volcanism? *Geochem. Geophys. Geosyst.* **4**, 1089 (2003).
- Sager, W. W. et al. Oceanic plateau formation by seafloor spreading implied by Tamu Massif magnetic anomalies. *Nat. Geosci.* **12**, 661–666 (2019).
- Kopp, H. et al. Fossil hot spot–ridge interaction in the Musicians Seamount Province: geophysical investigations of hot spot volcanism at volcanic elongated ridges. *J. Geophys. Res. Solid Earth* **108**, 2160 (2003).
- O’Connor, J. M. et al. Deformation-related volcanism in the Pacific Ocean linked to the Hawaiian–Emperor bend. *Nat. Geosci.* **8**, 393–397 (2015).
- Fletcher, M., Wyman, D. A. & Zahirovic, S. Mantle plumes, triple junctions and transforms: a reinterpretation of Pacific Cretaceous–Tertiary LIPs and the Laramide connection. *Geosci. Front.* **11**, 1133–1144 (2020).
- Davis, A. S., Gray, L. B., Clague, D. A. & Hein, J. R. The Line Islands revisited: new $^{40}\text{Ar}/^{39}\text{Ar}$ geochronologic evidence for episodes of volcanism due to lithospheric extension. *Geochem. Geophys. Geosyst.* **3**, 1–28 (2002).
- Sager, W. W. What built Shatsky Rise, a mantle plume or ridge tectonics? *Geol. Soc. Am. Spec. Pap.* **388**, 15 (2005).
- Heaton, D. E. & Koppers, A. A. P. High-resolution $^{40}\text{Ar}/^{39}\text{Ar}$ geochronology of the Louisville seamounts IODP expedition 330 drill sites: implications for the duration of hot spot-related volcanism and age progressions. *Geochem. Geophys. Geosyst.* **20**, 4073–4102 (2019).
- Bono, R. K., Tarduno, J. A. & Bunge, H.-P. Hotspot motion caused the Hawaiian–Emperor bend and LLSVPs are not fixed. *Nat. Commun.* **10**, 3370 (2019).
- Cande, S. C., Raymond, C. A., Stock, J. & Haxby, W. F. Geophysics of the Pitman Fracture Zone and Pacific–Antarctic plate motions during the Cenozoic. *Sci. New Ser.* **270**, 947–953 (1995).
- Wessel, P. & Kroenke, L. W. Pacific absolute plate motion since 145 Ma: an assessment of the fixed hot spot hypothesis. *J. Geophys. Res.* **113**, B06G101 (2008).

42. O'Connor, J. M. et al. Constraints on past plate and mantle motion from new ages for the Hawaiian–Emperor seamount chain. *Geochem. Geophys. Geosyst.* **14**, 4564–4584 (2013).
43. Staudigel, H., Koppers, A. A. P., Plank, T. A. & Hanan, B. B. Seamounts in the subduction factory. *Oceanography* **23**, 176–181 (2010).
44. Janney, P. E. & Castillo, P. R. Isotope geochemistry of the Darwin Rise seamounts and the nature of long-term mantle dynamics beneath the south central Pacific. *J. Geophys. Res. Solid Earth* **104**, 10571–10589 (1999).
45. Jackson, M. G. et al. The return of subducted continental crust in Samoan lavas. *Nature* **448**, 684–687 (2007).
46. Konter, J. G. et al. One hundred million years of mantle geochemical history suggest the retiring of mantle plumes is premature. *Earth Planet. Sci. Lett.* **275**, 285–295 (2008).
47. Hart, S. R. et al. Genesis of the Western Samoa seamount province: age, geochemical fingerprint and tectonics. *Earth Planet. Sci. Lett.* **227**, 37–56 (2004).
48. Price, A. A. et al. Distinguishing volcanic contributions to the overlapping Samoan and Cook–Austral hotspot tracks. *J. Petrol.* **63**, egac032 (2022).
49. Reinhard, A. A. et al. “Petit spot” rejuvenated volcanism superimposed on plume-derived Samoan shield volcanoes: evidence from a 645-m drill core from Tutuila Island, American Samoa. *Geochem. Geophys. Geosyst.* **20**, 1485–1507 (2019).
50. Staudigel, H. et al. The longevity of the South Pacific isotopic and thermal anomaly. *Earth Planet. Sci. Lett.* **102**, 24–44 (1991).
51. Stern, R. J., Fouch, M. J. & Klempner, S. L. in *Inside the Subduction Factory* (ed. Eiler, S.) 175–222 (American Geophysical Union, 2004).
52. DIGIS Team ‘2023-12-PVFZCE_IJU-BONIN-MARIANA_ARC.csv’. GEOROC compilation: convergent margins. GEOROC <https://doi.org/10.25625/PVFZCE/6MYFA2> (2023).
53. Torsvik, T. H. et al. Pacific–Panthalassic reconstructions: overview, errata and the way forward. *Geochem. Geophys. Geosyst.* **20**, 3659–3689 (2019).
54. Chandler, M. T. et al. Reconstructing Ontong Java Nui: implications for Pacific absolute plate motion, hotspot drift and true polar wander. *Earth Planet. Sci. Lett.* **331–332**, 140–151 (2012).
55. Davidson, P. C., Koppers, A. A. P., Sano, T. & Hanyu, T. A younger and protracted emplacement of the Ontong Java Plateau. *Science* **380**, 1185–1188 (2023).
56. Wei, X. et al. Co-occurrence of HIMU and EM1 components in a single Magellan seamount: implications for the formation of West Pacific Seamount Province. *J. Petrol.* **63**, egac022 (2022).
57. Harrison, L. N. & Weis, D. The size and emergence of geochemical heterogeneities in the Hawaiian mantle plume constrained by Sr–Nd–Hf isotopic variation over ~47 million years. *Geochem. Geophys. Geosyst.* **19**, 2823–2842 (2018).
58. Harrison, L. N., Weis, D. & Garcia, M. O. The link between Hawaiian mantle plume composition, magmatic flux, and deep mantle geodynamics. *Earth Planet. Sci. Lett.* **463**, 298–309 (2017).
59. Harrison, L. N., Weis, D. & Garcia, M. O. The multiple depleted mantle components in the Hawaiian–Emperor chain. *Chem. Geol.* **532**, 119324 (2020).
60. Bonneville, A., Dosso, L. & Hildenbrand, A. Temporal evolution and geochemical variability of the South Pacific superplume activity. *Earth Planet. Sci. Lett.* **244**, 251–269 (2006).
61. Buff, L. et al. “Missing links” for the long-lived Macdonald and Arago hotspots, South Pacific Ocean. *Geology* **49**, 541–544 (2021).
62. Hémond, C., Devey, C. W. & Chauvel, C. Source compositions and melting processes in the Society and Austral plumes (South Pacific Ocean): element and isotope (Sr, Nd, Pb, Th) geochemistry. *Chem. Geol.* **115**, 7–45 (1994).
63. Cheng, Q. et al. in *Seamounts, Islands, and Atolls* (eds Keating, B. H. et al.) 283–296 (American Geophysical Union, 1987).
64. Beier, C., Vanderkluyzen, L., Regelous, M., Mahoney, J. J. & Garbe-Schönberg, D. Lithospheric control on geochemical composition along the Louisville Seamount Chain. *Geochem. Geophys. Geosyst.* **12**, QOAM01 (2011).
65. DIGIS Team GEOROC compilation: ocean island groups. GEOROC <https://doi.org/10.25625/WFJZKY> (2023).
66. Tejada, M. L. G., Mahoney, J. J., Duncan, R. A. & Hawkins, M. P. Age and geochemistry of basement and alkalic rocks of Malaita and Santa Isabel, Solomon Islands, southern margin of Ontong Java Plateau. *J. Petrol.* **37**, 361–394 (1996).
67. Tejada, M. L. G. et al. Pin-pricking the elephant: evidence on the origin of the Ontong Java Plateau from Pb–Sr–Hf–Nd isotopic characteristics of ODP leg 192 basalts. *Geol. Soc. Lond. Spec. Publ.* **229**, 133–150 (2004).
68. Tejada, M. L. G., Mahoney, J. J., Neal, C. R., Duncan, R. A. & Petterson, M. G. Basement geochemistry and geochronology of Central Malaita, Solomon Islands, with implications for the origin and evolution of the Ontong Java Plateau. *J. Petrol.* **43**, 449–484 (2002).
69. Hoernle, K. et al. Age and geochemistry of volcanic rocks from the Hikurangi and Manihiki oceanic plateaus. *Geochim. Cosmochim. Acta* **74**, 7196–7219 (2010).
70. Timm, C. et al. Age and geochemistry of the oceanic Manihiki Plateau, SW Pacific: new evidence for a plume origin. *Earth Planet. Sci. Lett.* **304**, 135–146 (2011).
71. Ingle, S. et al. Depleted mantle wedge and sediment fingerprint in unusual basalts from the Manihiki Plateau, central Pacific Ocean. *Geology* **35**, 595 (2007).
72. Golowin, R. et al. Boninite-like intraplate magmas from Manihiki Plateau require ultra-depleted and enriched source components. *Nat. Commun.* **8**, 14322 (2017).
73. Hauri, E. H., Whitehead, J. A. & Hart, S. R. Fluid dynamic and geochemical aspects of entrainment in mantle plumes. *J. Geophys. Res.* **99**, 24275–24300 (1994).
74. Class, C. & Lehnert, K. PetDB expert MORB (mid-ocean ridge basalt) compilation <https://search.earthchem.org/> (2012).
75. Ruellan, E., Delteil, J., Wright, I. & Matsumoto, T. From rifting to active spreading in the Lau Basin–Havre Trough backarc system (SW Pacific): locking/unlocking induced by seamount chain subduction. *Geochem. Geophys. Geosyst.* **4**, 8909 (2003).
76. Torsvik, T. H., Steinberger, B., Gurnis, M. & Gaina, C. Plate tectonics and net lithosphere rotation over the past 150My. *Earth Planet. Sci. Lett.* **291**, 106–112 (2010).

Publisher's note Springer Nature remains neutral with regard to jurisdictional claims in published maps and institutional affiliations.

Springer Nature or its licensor (e.g. a society or other partner) holds exclusive rights to this article under a publishing agreement with the author(s) or other rightsholder(s); author self-archiving of the accepted manuscript version of this article is solely governed by the terms of such publishing agreement and applicable law.

© The Author(s), under exclusive licence to Springer Nature Limited 2025

Sample analysis for mantle source composition

Samples were collected with ROV *Deep Discoverer*, aboard the National Oceanic and Atmospheric Administration (NOAA) exploration vessel *Okeanos Explorer*, during expedition EX1606 to the Wake Island Unit of the US Pacific Remote Island Marine National Monument. Dive samples were cut open and the seven least-altered samples were selected. All compositional data for the Wake samples can be found in Extended Data Table 1.

Major elements were collected by laser-induced breakdown spectroscopy, using a Nd-YAG (neodymium-doped yttrium aluminum garnet) 20-mJ pulsed laser and a Catalina Scientific EMU-120 echelle spectrometer. Major element compositions were calibrated against 36 different standards, using partial least-squares regression, in MATLAB. Predicted compositions of unknown samples using partial least squares show typically <2 wt% variability on repeat analyses, after each sample is re-normalized to 100% total values.

Trace element data were obtained using a Thermo Finnegan Element2 ICP-MS (University of South Carolina). Aliquots of sample powders were lightly leached with 0.1 N hydrochloric acid (HCl) in a sonic bath for 20 min to mitigate any low-temperature overprinting by seawater without compromising the primary bulk composition. The sample powders were then dissolved in a Teflon-distilled HF:HNO₃ mixture, subsequently dissolved in 2 wt% HNO₃, and spiked with indium at 2-ppb concentration in the solution. The US Geological Survey reference material BHVO-2 was used as a standard and the reference materials BCR-2 and JB-2 were run as unknowns along the samples. The calculated concentrations for the unknowns agree well within 5% for most elements relative to the recommended concentrations from GeoReM (accessed August 2022⁷⁷).

Pb–Sr–Nd–hafnium (Hf) isotopic compositions were obtained following mechanical and chemical procedures to remove seafloor alteration contributions⁴ and previously detailed elemental separation procedures⁷⁸. In short, a small piece from the centre of each sample was crushed, altered pieces were removed by hand-picking, and the approximately 500–1,000-µm clean fraction was acid-leached in several steps, all done on a hot plate at about 80–100 °C: about 1 h each in 2 M HNO₃, 6 N HCl and 4 M HNO₃, before undergoing a final approximately 16-h leach in 6 N HCl. Samples were subsequently dissolved for sequential recovery of Sr, Pb, Nd and Hf. An aliquot of unleached BCR-2 powder was digested alongside the samples as a quality monitor and is reported in Supplementary Table 2. Pb was separated and purified with Sr-Spec resin and AG1-x8 resin, respectively⁷⁸. Isotope measurements were performed on a Nu Plasma high resolution multicollector inductively coupled plasma mass spectrometer (HR MC-ICP-MS) at the University of Hawai'i at Mānoa (Pb, except for EX1606-D3-3) using sample standard bracketing, and thallium doping to monitor fractionation. The repeatability of Pb isotope analysis of a given sample is typically about ±0.001 (absolute 2σ). Compositions were normalized to values⁷⁹ for National Institute of Standards and Technology (NIST) 981 Pb.

The Sr, Nd and Hf fractions of the same sample and standard digestions used for Pb isotopes were further processed at the University of South Carolina, but we note that Pb isotope data for sample EX1606-D3-3 were collected at the University of South Carolina using methods similar to those used at the University of Hawai'i at Mānoa and normalized to accepted NIST 981 values⁷⁹. Sr samples were purified with Sr-Spec resin in HNO₃. For Nd, the rare earth element fractions were separated from major element matrix using TRU spec resin in HNO₃ and HCl media, and Nd was separated from the other rare earth elements on an LN resin using 0.25 N HCl. Hf was isolated from the matrix on LN resin from the fractions recovered from the washes of the TRU spec column⁸⁰. A Thermo Finnegan NeptunePlus at University of South Carolina was used for remaining (Sr, Nd and Hf (ref. 81)) isotope analyses. Repeated analyses of SRM987 dispersed with the samples gave ⁸⁷Sr/⁸⁶Sr = 0.710321 ± 0.000007, (2σ, n = 11). The data are reported

relative to the recommended SRM987 ⁸⁷Sr/⁸⁶Sr_{SRM987} = 0.71025. Nd isotopes were corrected for fractionation using ¹⁴⁶Nd/¹⁴⁴Nd = 0.7219 and repeated analyses of the JNdi-1 reference material yielded an average ¹⁴³Nd/¹⁴⁴Nd = 0.512102 ± 0.000005 (2σ, n = 11). The Nd data are reported relative to the accepted value for JNdi-1 of ¹⁴³Nd/¹⁴⁴Nd = 0.512115. Hf isotopes were corrected for fractionation using ¹⁷⁹Hf/¹⁷⁷Hf = 0.7325. An in-house Hf standard solution was determined at ¹⁷⁶Hf/¹⁷⁷Hf = 0.282142 ± 0.000006 (2σ, n = 8), which corresponds to the original JMC 475 solution value of ¹⁷⁶Hf/¹⁷⁷Hf = 0.282163. The data are reported relative to the accepted JMC 475 value of ¹⁷⁶Hf/¹⁷⁷Hf = 0.282160 (ref. 82). BCR-2 duplicates are duplicate analyses of the same digestion.

Results and brief sample characterizations, including age-corrected isotopic ratios for the Wake samples based on successful age determinations (see next section for details), are reported in Extended Data Table 1. Six of the samples reported here are consistent with the interpretation that they originated from the Rurutu–Arago hotspot. The seventh sample (D13-1) has an age of 164 Ma (Supplementary Table 3) and is too old to have originated from the Rurutu–Arago hotspot by about 70 Myr and is more likely related to seafloor formation. The isotopic behaviour shown in Extended Data Figs. 3 and 4 shows the compositional agreement between the samples characterized here, and published data for the Rurutu–Arago hotspot track.

Sample analysis for ⁴⁰Ar/³⁹Ar geochronology

⁴⁰Ar/³⁹Ar age determination experiments were conducted at the Oregon State University Argon Geochronology Laboratory using incremental carbon dioxide (CO₂) laser heating and analysis using a multi-collector ARGUS-VI noble gas mass spectrometry. Preferred lava flow samples were chosen based on petrographic analyses, focusing on phenocryst abundances and relative degree of alteration. Samples that contained fresh phenocrystic phases (clinopyroxene and plagioclase) were preferentially chosen. In the absence of phenocrysts, groundmass was selected for ⁴⁰Ar/³⁹Ar analyses. When available, multiple phases from a single lava flow were analysed to test for age reliability. Rocks were crushed and sieved to grain size fractions of 100–180 µm for the most altered samples and 180–250 µm for fresher and coarser phenocryst phases. These fractions were washed in deionized water and dried in a 50 °C oven overnight. Next, target phases were concentrated using a Frantz magnetic separator. The crushate were then leached with 1-h sonic baths in 1 N HCl, 6 N HCl, 1 N HNO₃ and 3 N HNO₃ with thorough rinsing and sonication in deionized water between each bath. Plagioclase was subsequently leached twice in 5% HF for 5 min and clinopyroxene samples were additionally leached once in 15% HF for 15 min. The groundmass crushate was divided into three aliquots: (1) no HF treatment; (2) 5% HF for 90 s; (3) 5% HF for 3 min. All samples were then sonicated in ultrapure water for 1 h. Samples were dried at 50 °C in an oven overnight then handpicked under a binocular microscope to achieve pure and homogeneous mineral separates.

Approximately 2–50 mg of each separate was packed into aluminium capsules for irradiation. Fish Canyon Tuff sanidine was used as a flux monitor loaded at the bottom, top and between every three sample packets. The sample columns were irradiated for 6 h in the CLICIT position of Oregon State University's TRIGA nuclear reactor. Incremental heating experiments consisted of 20–30 steps for phenocrysts and 50–60 steps for groundmass separates. Blanks were measured at the beginning, end, and every two or three incremental heating steps.

Experiments consisted of loading 2–25 mg of individual samples into a copper tray, which were then brought under an ultrahigh vacuum. Samples were pre-cleaned using a defocused 30-W Synrad CO₂ laser beam at low power to release adhered atmospheric gas. Separates were then heated by scanning the CO₂ laser beam over the separates for 60 s using incrementally higher laser power. Gas was processed using three getters held at approximately 450 °C, 250 °C and 20 °C for a total of 3 min for plagioclase and 6 min for clinopyroxene and groundmass. Five masses were analysed simultaneously using a Thermo Fisher Scientific multi-collector ARGUS-IV mass spectrometer with 40

measured on a $10^{12}\text{-}\Omega$ Faraday cup, 39, 38 and 37 on $10^{13}\text{-}\Omega$ Faraday cups, and 36 on an ion-counting CuBe electron multiplier. Ages were calculated using ArArCALC v2.7.0⁸³. All ages are normalized to Fish Canyon Tuff sanidine age of 28.201 ± 0.046 Ma (2σ) using a decay constant of $5.530 \pm 0.097 \times 10^{-10} \text{ yr}^{-1}$ (2σ)^{84,85}. Air standards were analysed to obtain mass discrimination factors using an atmospheric $^{40}\text{Ar}/^{36}\text{Ar}$ value of 298.56 ± 0.31 (0.104%)⁸⁶. Refer to the next section for other correction factors used during sample calculations.

Age results

Four of the seven samples reported in this study were chosen for $^{40}\text{Ar}/^{39}\text{Ar}$ age determination experiments based on petrographic analysis: EX1606-D3-3, EX1606-D10-1, EX1606-D12-1 and EX1606-D13-1. Here we determine whether an age experiment is concordant if it incorporates 50% or more of the cumulative $^{39}\text{Ar}\%$ released within the plateau and the steps are reasonably concordant provided the age and alteration state of the submarine lava flows. For phases with more than one experiment, ages are stacked such that the individual heating steps are combined into one large experiment. EX1606-D10-1 and EX1606-D12-1 did not produce age results in line with community guidelines, and thus are not considered here. However, phenocryst separates from EX1606-D3-3 and plagioclase separates from EX1606-D13-1 produced reliable eruption age determinations (Extended Data Fig. 11).

Plagioclase separates from EX1606-D3-3 yielded a plateau age of 91.21 ± 0.17 Myr (2σ ; $n = 2$; Extended Data Fig. 11a). The inverse isochron indicates $^{40}\text{Ar}/^{36}\text{Ar}_{\text{initial}}$ of 287.51 ± 33.77 , within uncertainty of atmospheric values (298.56 (ref. 86)). Correspondingly, the inverse isochron and plateau age determinations are within error of one another. The plateau age of the clinopyroxene separate from the same sample (91.68 ± 14.61 Ma, 2σ ; $n = 1$; Extended Data Fig. 11c) agrees with the plagioclase age determination but has high uncertainty owing to low potassium abundance. One step in both the clinopyroxene and plagioclase experiments suggests anomalously low ages, which are probably the degassing of melt inclusions and not representative of eruption timing. As the plateau is continuous before and after the heating step with anomalous apparent ages, they are excluded from the plateau calculation. Although we prefer the plagioclase age determination owing to the high resolution, an age of 91 Ma is further supported by the clinopyroxene age determination.

Plagioclase separates from EX1606-D13-1 yielded a plateau age determination of 164 ± 0.29 Ma (2σ ; $n = 1$; Extended Data Fig. 11d). The inverse isochron age (163.72 ± 0.23 Ma; $n = 1$; Extended Data Fig. 11e) is within error of the plateau age determination and has an intercept that is similar to atmospheric ($^{40}\text{Ar}/^{36}\text{Ar}_{\text{initial}}$: 308 ± 33.44). The three groundmass separates from D13-1 (Extended Data Fig. 11f) produced age spectrums that do not meet the statistical criteria for a reliable age determination⁸⁷ but generally support the Middle Jurassic age inferred from the corresponding concordant plagioclase separate.

Isotopic colour-coding for finger-printing

To show the compositional distinction between the hotspot tracks in the western Pacific, as well as to show how compositions backtrack around present-day hotspots, the radiogenic isotope composition of the tracks are colour-coded^{14,17,46}. The technique focuses on use of $^{87}\text{Sr}/^{86}\text{Sr}$ – $^{143}\text{Nd}/^{144}\text{Nd}$ – $^{206}\text{Pb}/^{204}\text{Pb}$ isotope compositions, because principal component analysis shows that these represent the largest compositional variations in hotspots^{47,88}. In this space, hotspots scatter between four extreme end-member compositions: HIMU, EMI, EMII and DMM⁸⁹. Each hotspot's samples define an elongated, prolate ellipsoid, and these ellipsoids (32 in the global hotspot database) radiate from a central region, known as FOZO⁷³ or C (common component)⁹⁰. The colour-coding⁴⁶ assigns a level of colour-saturation based on its distance from this centre, and the colour depends on the end-member that a particular sample trends closest to (Fig. 1, inset). Compositions that are on the trend towards an end-member but cannot be resolved

from the central FOZO⁷³ or C⁹⁰ component are coloured grey (it is noted that the cut-off percentages for each end-member are shown on the colour bars in Fig. 1, inset). Using this colour-coding approach results in dominantly blue to blue–grey colouration for symbols, representing HIMU compositions most commonly sampled by the plume, which dominate the hotspot track that runs from the Cook–Austral islands in the central equatorial Pacific to seamount tracks in the western Pacific. This HIMU compositional ‘signature band’ in map view (that is, as the blue-dominant symbols that represent the Rurutu–Arago HIMU hotspot track form a ‘band’ across the south Pacific and into the Western Pacific Seamount Province) is consistent with predicted APM in the Pacific until at least 80 Ma, and forms the basis for our investigation that links the Wake-area seamounts in the western Pacific to the long-lived Rurutu–Arago hotspot that also includes the Tuvalu islands and the Gilbert Ridge seamount track. In addition, the red (representing EM2) and green (EM1) compositional colour-coding for Samoa appears in young Samoan hotspot lavas and also appears in the far western Pacific in the Cretaceous Magellan seamounts. Recent work in Samoa has shown a temporal compositional evolution from red (EM2) to green (EM1), representing the evolution from shield to rejuvenated stage of volcanism at Samoa, and the same is observed in the western Pacific when compositions and ages are assessed (Hemler and Vlinder seamounts^{4,91}; Extended Data Fig. 9). The effects of seawater alteration processes^{92,93}, plume–ridge interaction^{94,95} and model isotopic ingrowth corrections^{14,96–98} are discussed further in Supplementary Information.

APM modelling

Although initial models^{2,99} already showed that simple plate rotations do fit the shapes of several hotspot tracks, recent models⁴¹ have evolved to include more sophisticated techniques to find the best-fit APM models by using multiple hotspots and by resolving continuous plate rotations from both seamount locations and ages. In addition, some models include large-scale mantle flow, comparisons between ocean basins and plume motion^{6,40,100,101}. For the Pacific plate >80 Ma, few data are available as neither Hawai'i nor Louisville continue past 80 Ma (refs. 102,103), and plate circuits that would allow comparison with the Indo-Atlantic hotspot do not extend beyond this time either⁶. In most existing models, the time period before 80 Ma is populated with data from Shatsky Rise and the Mid-Pacific Mountains, but their respective structures were within about 1,000 km of a ridge system¹⁰⁴ (Extended Data Fig. 1) and during their formation these tracks are likely to have been influenced by ridge interaction^{37,104}. However, the Rurutu–Arago and Samoa hotspots do define tracks in this age range that are clearly distinct in their isotopic compositions (Fig. 1; see the section on colour-coding) and that are truly intraplate before 80 Ma (Extended Data Fig. 1). We conclude that Rurutu–Arago and Samoa therefore are a more faithful reflection of APM for the Pacific Plate before 80 Ma.

The presence of two hotspot tracks—Samoa and Rurutu–Arago—provides a means to fit a plate rotation for 80–100 Ma that fits both hotspots, thereby relying on their common motion to define an APM pole for that period. Unlike younger volcanic tracks, Samoa and Rurutu–Arago provide enough data to outline the overall hotspot track; however, the sample and data density are low, such that constraints are lacking for a high-resolution model⁴¹. Instead, the available data here are used to identify an 80–100-Ma section in both hotspot tracks (Extended Data Fig. 8 and Extended Data Tables 1 and 2), after which a least-squares method is used to find the best-fit rotation pole that satisfies the morphological trends in both seamount trails. The method¹⁸ consists of finding the best-fit pole that minimizes the variance in calculated angular (seamount to pole) distances, in the least-squares sense. The solution is found with a grid-search algorithm that tests

$$\text{var}(d_{ij}) = \sum_{j=1}^M \sum_{i=1}^N \frac{(d_i^j - d_{\text{mean}}^j)^2}{N}$$

which calculates the variance in distance (d) for all seamounts in the 80–100-Ma hotspot track segment relative to the mean distance for a given hotspot (d_{mean}). Variables M and N are the dimensions of the grid over which the search is performed, with grid values iteratively evaluated at each position within the grid, defined by j and i . The variation in distance per hotspot is normalized by the number of seamounts (N) per hotspot in that particular track segment. This technique suggests a best-fit stage pole west of the Samoa-related seamounts, near the Equator (0.7° S, 315.7° E; rotation rate 0.975° Myr $^{-1}$; Extended Data Table 1). The resulting K01m APM model is a much better fit to the two hotspot tracks, particularly for the Rurutu–Arago hotspot, where the predicted track now bends sharply to the west at about 100 Ma, just northwest of Wake Island (Fig. 1 and Extended Data Figs. 7 and 9). Owing to the shift in the rotation pole compared with previous models, the angular distance from the pole to the Rurutu–Arago track and this rotation rate provide a better fit to the seamount trails. Despite these improvements, several issues must be considered before this model can be applied to the Louisville hotspot track.

Plate motion southeast of the OJP involved more than just the Pacific Plate. During the break-up of the OJP–Nui, the Manihiki and Hikurangi plates formed, and the Chazca Plate resided immediately to the east⁵³. It is important to evaluate whether these plates moved independently with respect to the Pacific Plate when the Ellice Basin was located over the Louisville hotspot. The relevant plates and microplates are associated with the break-up of the OJP–Nui. The oldest Louisville seamounts (ranging in age from 1 Ma to 79 Ma (refs. 8,38)) are located south of the Osbourn Trough and west of the Wishbone Scarp, representing a small plate forming as Hikurangi separated from the OJP. However, true spreading on the Osbourn Trough may have ceased between 101 Ma and 100 Ma (refs. 105,106). Any further rotation of this plate ceased between about 84 Ma and 79 Ma (refs. 107–109), so Louisville seamounts younger than 79 Ma formed after this plate was already part of the Pacific Plate. Thus, Louisville seamounts after 79 Ma properly represent Pacific Plate motion with respect to the Louisville hotspot. The only other area where older volcanoes related to Louisville may be exposed is in the area of the Ellice Basin between the OJP and Manihiki¹⁴. However, the exact timing of cessation of motion between the separating plateaus is not well constrained²¹. The sparse age information¹⁰⁹ from the Ellice Basin includes the 95-Ma Foumatua Seamount located on the fossil ridge system¹⁴, constraining a minimum age of about 95 Ma for when seafloor spreading in the Ellice Basin shut down, as suggested by models based on the seafloor fabric¹¹⁰. Critically, Foumatua Seamount is part of a group of similarly aged ‘Ellice Basin seamounts’ that have an isotopic composition that overlaps with that of the younger Louisville seamounts¹⁴ (Fig. 2). These seamounts are located where our APM model predicts the Louisville hotspot around 95 Ma, and the seamounts are also age-progressive with the Louisville seamounts (Figs. 1 and 2). The 115-Ma Seka Seamount, located north of the Ellice Basin fossil ridge and near the southern terminus of Gilbert Ridge several hundred kilometres east of the OJP, places the underlying seafloor—and westwards motion of the OJP fragment relative to the plume—at a minimum age of 115 Ma, thus indicating that early stage Ellice Basin opening was rapid¹⁰⁹, and potentially even triggered by the voluminous melting of the Louisville plume head at that time, much like the inferred fossil plume head-ridge system at Tamu Massif³².

Owing to the known wide variation in palaeomagnetic latitude estimates for the OJP⁵⁴, any microplate considerations before about 100 Ma are under-constrained at best. Either the plateaus rotated around the time of break-up⁵⁴ or the OJP was already fixed with respect to the Pacific Plate¹⁰⁸. Regardless, the sheer size of the entire OJP–Nui combined structure is so large that neither a rotation of the plateaus nor ongoing spreading in the Ellice Basin until about 100 Ma would place the predicted Louisville hotspot outside of the outline of the combined OJP–Nui plateau (or even the OJP by itself) at 120 Ma (Fig. 3). This is mainly owing to the final east–west length of the 100–120-Ma

predicted Louisville hotspot track being shorter than the width of the OJP, which is thought to have largely moved east–west^{21,110} (Fig. 1). In Fig. 3, the approximate eruptive locations are also shown assuming the OJP either was fixed from about 120 Ma or only rotated around a pole internal to the plateau⁵⁴. Intriguingly, the rotation of the plateaus places the eruptive location at about 120 Ma near the triple junction between the three plateaus.

Backtracking

Individual volcanoes with age determinations can be backtracked to their original eruptive location, by rotating present-day volcano locations in the opposite direction of plate motion, according to the sequence of APM model rotations. Existing APM models are used as stage pole rotations to accommodate volcanic ages in between supplied finite rotations. Instead of each volcano backtracking to the same single hotspot location, this process generates clusters owing to various geologic and measurement uncertainties, such as: (1) volcanic age precision and accuracy, (2) extended eruption of single volcanoes (up to 7 Ma (ref. 111)), (3) offset between sampled rift zone eruptions and the central crater, and (4) lithospheric structure offsetting volcano from mantle source^{4,112}. Cumulatively, these uncertainties could cause hundreds of kilometres of scatter in backtracked locations that cluster around the present-day hotspot⁴⁶.

Two categories of structures were backtracked here: (1) individual volcanoes of Rurutu–Arago, Samoa and Louisville, and (2) the OJP as a single structure. For the individual hotspot volcanoes (Extended Data Table 2), published ⁴⁰Ar/³⁹Ar ages were used^{9,113–117}, and symbols for reconstructed volcanoes are coloured (see the section on colour-coding) based on their isotopic composition^{10–12,14,45}. This highlights the compositional groups by colour, matching present-day hotspot locations at Samoa and Rurutu–Arago, as well as Macdonald and Rarotonga for reference. Moreover, the probability density function of backtracked locations (constructed with a Gaussian kernel) shows four peaks in the distribution that also correspond to the same four present-day hotspots (Extended Data Fig. 8). In addition to the density estimates, a running mean can also be calculated for the backtracked locations and related sample ⁴⁰Ar/³⁹Ar ages. These ‘age tracks’ represent a smoothed estimate of how the hotspot source moved in time, with respect to the applied APM model, which can be thought of a proxy for plume motion in that reference frame. The results for the various models emphasize the tighter scattering (in blue-to-grey HIMU composition around Rurutu–Arago, red–green around Samoa) and shorter plume motion tracks for the K01m model. This result implies the least amount of plume motion is required for these models, whereas models that allow for plume motion require a significant amount, but also match predicted plume motion^{6,100} back to about 50 Ma for Hawai‘i and Louisville (Extended Data Fig. 8). As there are no plate circuits >80 Ma to enable comparison with the Indo-Atlantic hotspot reference frame⁴⁰, the modelling results can only be tested against Pacific hotspots.

Although testing the model against Rurutu–Arago and Samoa constraints is potentially circular, backtracking the OJP constitutes a more interesting test, as it was previously shown to backtrack 1,200 km away from the closest hotspot at 120 Ma, that is, Louisville¹. By defining the outline of the plateau as a series of individual points¹¹⁸, each individual point is backtracked with the updated K01m APM model. The result shows that the backtracked OJP plateau outline is located directly over the present-day Louisville hotspot (Extended Data Fig. 9). Similarly, the backtracked individual Louisville seamounts are also located over the present-day Louisville hotspot. The updated K01m model thus resolves the north–south discrepancy between modelling predictions of the eruptive location of the OJP and the track of Louisville. The conclusions for a 120-Ma OJP formation also hold for a slightly younger age of formation, recently suggested to be about 116 Ma (ref. 55). In this case, the modelled Louisville hotspot and Eastern Salient of the OJP are still closely spatially associated with each other at about 116 Ma. The revised

OJP formation age is similar to that of Seka Seamount, which would further suggest that OJP-Nui formation and initiation of Ellice Basin rifting were simultaneous events. This model represents a fixed-hotspot model, while multiple lines of evidence suggest hotspot sources to be mobile⁵. However, motion estimates for Louisville hotspot are within error of its location until at least about 70 Ma (refs. 8,9), and older data for the greater OJP-Nui are too variable to constrain any possible plume motion. Regardless of a lack of tight palaeolatitude constraints, the size of greater OJP-Nui allows for hundreds to thousands of kilometres of plume motion superimposed on our model, while still maintaining the 'end' of the Louisville hotspot track within its outline.

Data availability

All data generated during this study are included in this published article and its Supplementary Information files, and are available in the EARTH-CHEM repository (<https://doi.org/10.60520/IEDA/113695>). Source data are provided with this paper.

Code availability

The best-fit plate rotation MATLAB code is available upon request from the corresponding author.

77. Jochum, K. P. et al. GeoReM: a new geochemical database for reference materials and isotopic standards. *Geostand. Geoanal. Res.* **29**, 333–338 (2005).
78. Konter, J. G. & Storm, L. P. High precision ⁸⁷Sr/⁸⁶Sr measurements by MC-ICP-MS, simultaneously solving for Kr interferences and mass-based fractionation. *Chem. Geol.* **385**, 26–34 (2014).
79. Todt, W., Cliff, R., Hanser, A. & Hofmann, A. Evaluation of a ²⁰²Pb–²⁰⁵Pb double spike for high-precision lead isotope analysis. *Geophys. Monogr. Ser.* **95**, 429–437 (1996).
80. Münker, C., Weyer, S., Scherer, E. & Mezger, K. Separation of high field strength elements (Nb, Ta, Zr, Hf) and Lu from rock samples for MC-ICPMS measurements. *Geochim. Geophys. Geosyst.* **2**, 1064 (2001).
81. Béguelin, P., Bizimis, M., Beier, C. & Turner, S. Rift–plume interaction reveals multiple generations of recycled oceanic crust in Azores lavas. *Geochim. Cosmochim. Acta* **218**, 132–152 (2017).
82. Blichert-Toft, J. & Albarède, F. The Lu–Hf isotope geochemistry of chondrites and the evolution of the mantle–crust system. *Earth Planet. Sci. Lett.* **148**, 243–258 (1997).
83. Koppers, A. A. P. ArArCALC—software for ⁴⁰Ar/³⁹Ar age calculations. *Comput. Geosci.* **28**, 605–619 (2002).
84. Min, K., Mundil, R., Renne, P. R. & Ludwig, K. R. A test for systematic errors in ⁴⁰Ar/³⁹Ar geochronology through comparison with U/Pb analysis of a 1.1-Ga rhyolite. *Geochim. Cosmochim. Acta* **64**, 73–98 (2000).
85. Kuiper, K. F. et al. Synchronizing rock clocks of Earth history. *Science* **320**, 500–504 (2008).
86. Lee, J.-Y. et al. A redetermination of the isotopic abundances of atmospheric Ar. *Geochim. Cosmochim. Acta* **70**, 4507–4512 (2006).
87. Schaen, A. J. et al. Interpreting and reporting ⁴⁰Ar/³⁹Ar geochronologic data. *GSA Bull.* **133**, 461–487 (2021).
88. Allègre, C. J., Hamelin, B., Provost, A. & Dupré, B. Topology in isotopic multispace and origin of mantle chemical heterogeneities. *Earth Planet. Sci. Lett.* **81**, 319–337 (1987).
89. Zindler, A. & Hart, S. Chemical geodynamics. *Annu. Rev. Earth Planet. Sci.* **14**, 493–571 (1986).
90. Hanan, B. B. & Graham, D. W. Lead and helium isotope evidence from oceanic basalts for a common deep source of mantle plumes. *Sci. New Ser.* **272**, 991–995 (1996).
91. Smith, W. H. F., Staudigel, H., Watts, A. B. & Pringle, M. S. The Magellan seamounts: Early Cretaceous record of the South Pacific isotopic and thermal anomaly. *J. Geophys. Res. Solid Earth* **94**, 10501–10523 (1989).
92. Hauff, F., Hoernle, K. & Schmidt, A. Sr–Nd–Pb composition of Mesozoic Pacific oceanic crust (site 1149 and 801, ODP leg 185): implications for alteration of ocean crust and the input into the Izu–Bonin–Mariana subduction system. *Geochem. Geophys. Geosyst.* **4**, 8913 (2003).
93. Geldmacher, J. et al. The effects of submarine alteration and phosphatization on igneous rocks: implications for Sr-, Nd-, Pb-isotope studies. *Chem. Geol.* **631**, 121509 (2023).
94. Kingsley, R. H., Blichert-Toft, J., Fontignie, D. & Schilling, J.-G. Hafnium, neodymium, and strontium isotope and parent–daughter element systematics in basalts from the plume–ridge interaction system of the Salas y Gomez Seamount Chain and Easter Microplate. *Geochem. Geophys. Geosyst.* **8**, Q04005 (2007).
95. Regelous, M. Geochemistry of lavas from the Emperor seamounts, and the geochemical evolution of Hawaiian magmatism from 85 to 42 Ma. *J. Petrol.* **44**, 113–140 (2003).
96. Nebel, O. et al. Coupled Hf–Nd–Pb isotope co-variations of HIMU oceanic island basalts from Mangaia, Cook–Austral islands, suggest an Archean source component in the mantle transition zone. *Geochim. Cosmochim. Acta* **112**, 87–101 (2013).
97. Sun, S.-S. & McDonough, W. F. Chemical and isotopic systematics of oceanic basalts: implications for mantle composition and processes. *Geol. Soc. Lond. Spec. Publ.* **42**, 313–345 (1989).
98. Hart, S. R. & Blusztajn, J. Age and geochemistry of the mafic sills, ODP site 1276, Newfoundland margin. *Chem. Geol.* **235**, 222–237 (2006).
99. Morgan, W. J. Deep mantle convection plumes and plate motions. *AAPG Bull.* **56**, 203–213 (1972).
100. Steinberger, B., Sutherland, R. & O’Connell, R. J. Prediction of Emperor–Hawaii seamount locations from a revised model of global plate motion and mantle flow. *Nature* **430**, 167–173 (2004).
101. Müller, R. D. et al. A global plate model including lithospheric deformation along major rifts and orogens since the Triassic. *Tectonics* **38**, 1884–1907 (2019).
102. Duncan, R. A. & Keller, R. A. Radiometric ages for basement rocks from the Emperor seamounts, ODP leg 197. *Geochem. Geophys. Geosyst.* **5**, Q08L03 (2004).
103. Koppers, A. A. P., Duncan, R. A. & Steinberger, B. Implications of a nonlinear ⁴⁰Ar/³⁹Ar age progression along the Louisville seamount trail for models of fixed and moving hot spots. *Geochem. Geophys. Geosyst.* **5**, Q06L02 (2004).
104. Seton, M. et al. Global continental and ocean basin reconstructions since 200 Ma. *Earth Sci. Rev.* **113**, 212–270 (2012).
105. Hochmuth, K., Gohl, K. & Uenzelmann-Neben, G. Playing jigsaw with large igneous provinces—a plate tectonic reconstruction of Ontong Java Nui, West Pacific. *Geochem. Geophys. Geosyst.* **16**, 3789–3807 (2015).
106. Zhang, G.-L. & Li, C. Interactions of the Greater Ontong Java mantle plume component with the Osborn Trough. *Sci. Rep.* **6**, 37561 (2016).
107. Wobbe, F., Gohl, K., Chambord, A. & Sutherland, R. Structure and breakup history of the rifted margin of West Antarctica in relation to Cretaceous separation from Zealandia and Bellingshausen plate motion. *Geochem. Geophys. Geosyst.* **13**, Q04W12 (2012).
108. Mortimer, N. et al. Late Cretaceous oceanic plate reorganization and the breakup of Zealandia and Gondwana. *Gondwana Res.* **65**, 31–42 (2019).
109. Davidson, P. C., Koppers, A. A. P. & Konter, J. G. Rapid formation of the Ellice and Osborn basins and Ontong Java Nui breakup kinematics. *Geochem. Geophys. Geosyst.* **24**, e2022GC010592 (2023).
110. Benyshok, E. K., Wessel, P. & Taylor, B. Tectonic reconstruction of the Ellice Basin. *Tectonics* **38**, 3854–3865 (2019).
111. Konter, J. G. et al. Geochemical stages at Jasper Seamount and the origin of intraplate volcanoes. *Geochem. Geophys. Geosyst.* **10**, Q02001 (2009).
112. Koppers, A. A. P. Asynchronous bends in Pacific seamount trails: a case for extensional volcanism? *Science* **307**, 904–907 (2005).
113. Hart, S. R., Hauri, E. H., Oschmann, L. A. & Whitehead, J. A. Mantle plumes and entrainment: isotopic evidence. *Science* **256**, 517–520 (1992).
114. Koppers, A. A. P. et al. Samoa reinstated as a primary hotspot trail. *Geology* **36**, 435 (2008).
115. Koppers, A. A. P., Staudigel, H., Wijbrans, J. R. & Pringle, M. S. The Magellan seamount trail: implications for Cretaceous hotspot volcanism and absolute Pacific Plate motion. *Earth Planet. Sci. Lett.* **163**, 53–68 (1998).
116. Koppers, A. A. P. Mantle plumes persevere. *Nat. Geosci.* **4**, 816–817 (2011).
117. Koppers, A. A. P. et al. Age systematics of two young en echelon Samoan volcanic trails. *Geochem. Geophys. Geosyst.* **12**, Q07025 (2011).
118. Coffin, M. F. et al. Large igneous provinces and scientific ocean drilling: status quo and a look ahead. *Oceanography* **19**, 150–160 (2006).
119. Regelous, M. et al. Mantle dynamics and mantle melting beneath Niuafo’ou Island and the northern Lau back-arc basin. *Contrib. Mineral. Petrol.* **156**, 103–118 (2008).

Acknowledgements This work was supported by NOAA OER and GFOE, and is part of NSF-OCE project 1912934 to J.G.K. and P.W. A.A. was supported by NSF-REU grant 1560196 to P.W. M.G.J. was supported by NSF-OCE project 1912931. A.A.P.K. was supported by NSF-OCE 1912932. We thank the crew and the team of ROV pilots and engineers aboard the E/V *Okeanos Explorer* during the EX1606 expedition. This paper is dedicated to the memories of our first author, Jasper G. Konter, and our co-author, Paul Wessel.

Author contributions J.G.K. and V.A.F. contributed equally to this study. Conceptualization: J.G.K., V.A.F., M.G.J. and A.A.P.K. Field expedition and sampling: C.K. and J.G.K. Sample preparation and data collection: A.A., J.G.K., M.B. and S.B. Modelling: J.G.K., P.W. and A.A.P.K. Writing, editing and figures (original draft): all authors. Writing, editing, modelling and figures (revised version): V.A.F., K.K., M.G.J. and A.A.P.K.

Competing interests The authors declare no competing interests.

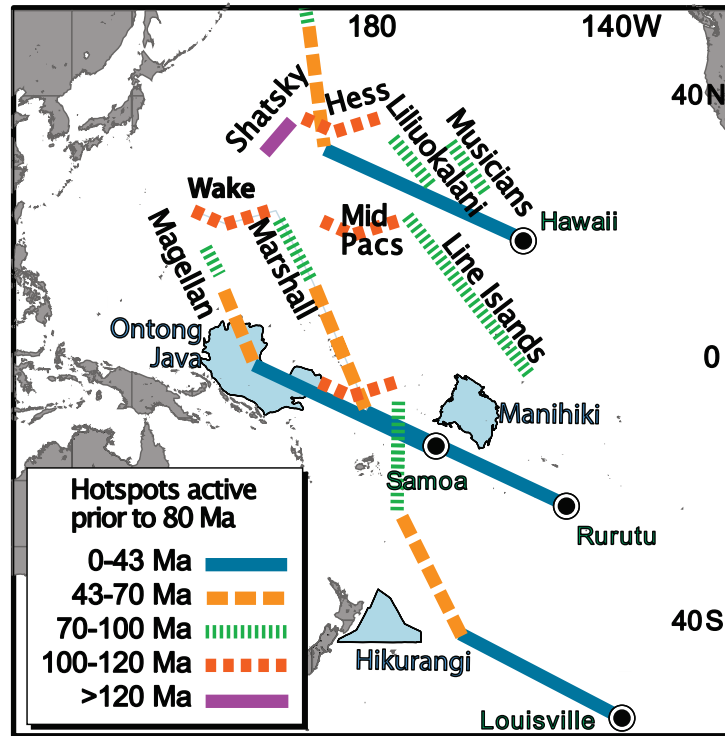
Additional information

Supplementary information The online version contains supplementary material available at <https://doi.org/10.1038/s41586-025-08889-0>.

Correspondence and requests for materials should be addressed to V. A. Finlayson.

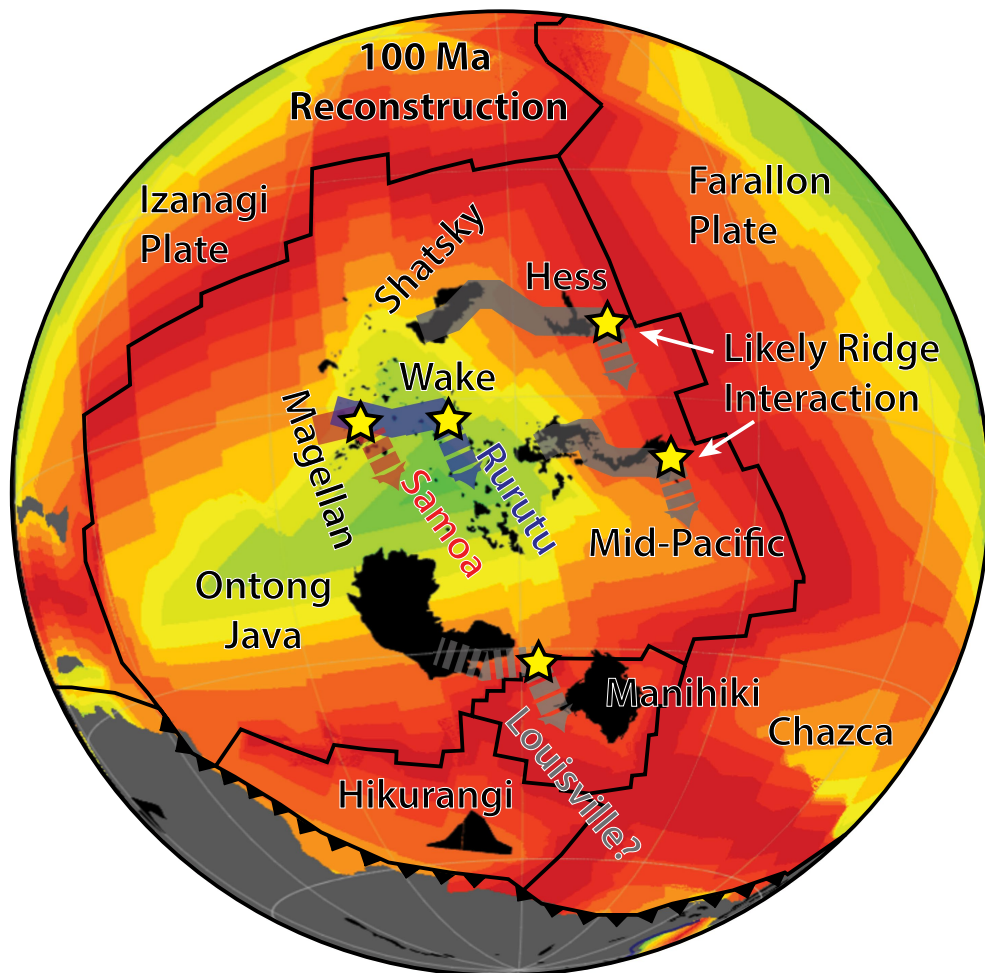
Peer review information *Nature* thanks Joann Stock and the other, anonymous, reviewer(s) for their contribution to the peer review of this work. Peer reviewer reports are available.

Reprints and permissions information is available at <http://www.nature.com/reprints>.

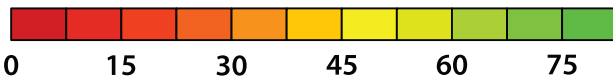


Extended Data Fig. 1 | Idealized map of the Pacific Ocean basin, showing relevant hotspot tracks, anchored at present-day locations indicated with black dots. Different sections of the hotspot tracks are color-coded by approximate range in eruption ages¹⁸. In the West Pacific, many sections are

represented by seamount groups known by their own names. In light blue, the three oceanic plateaus are shown that are thought to have made up Ontong-Java Nui together.

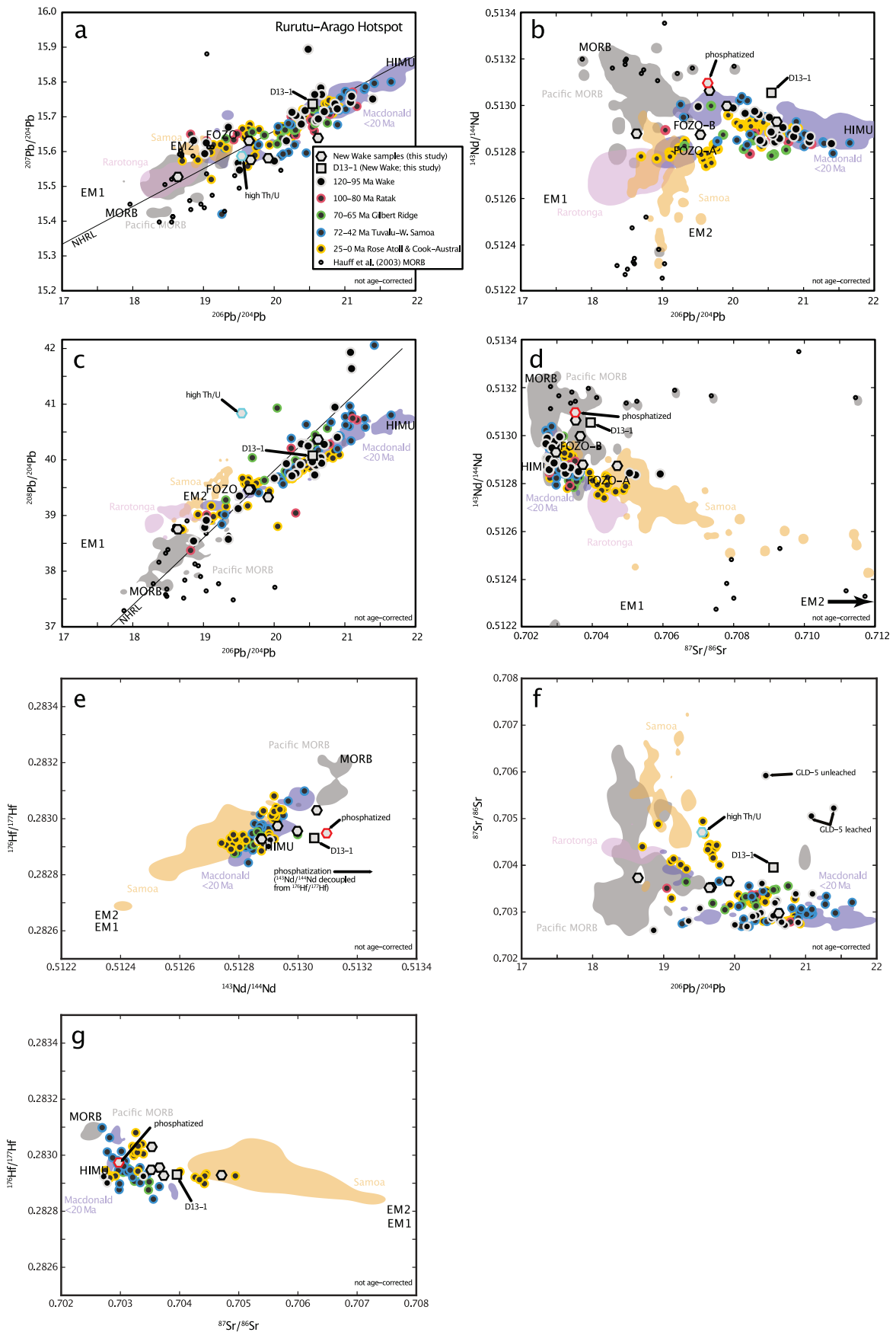


Crustal Age (Myr at time of reconstruction)



Extended Data Fig. 2 | 100 Ma plate configuration and relative position of volcanic structures relevant to APM modeling (global projection from GPlates¹⁰¹). Shatsky Rise and Mid-Pacific Mountains erupted near a spreading

center (likely causing plume motion⁵), while Rurutu-Arago and Samoa erupted within the growing Pacific plate. Louisville's position shows the approximate modeled track for the updated model rotation.

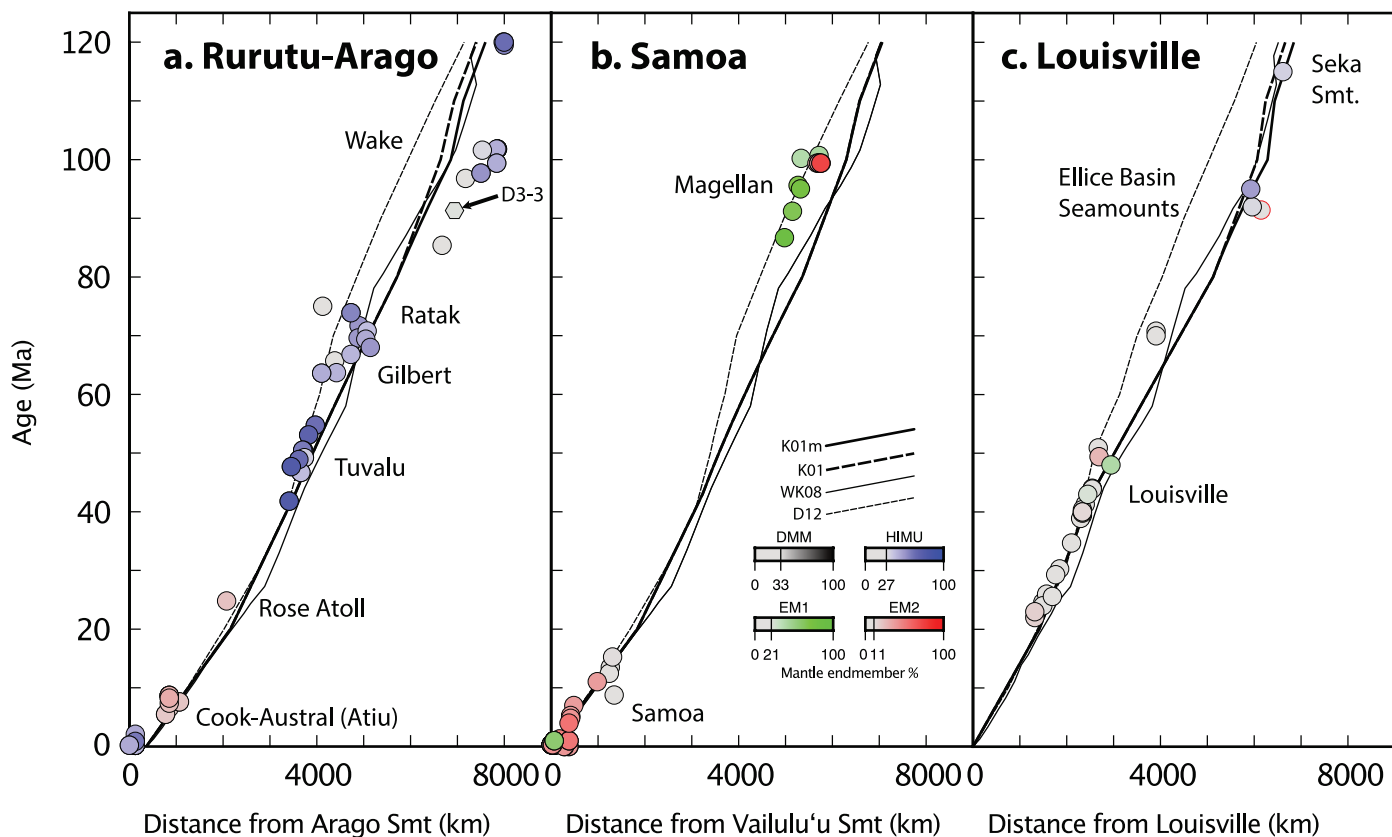


Extended Data Fig. 3 | See next page for caption.

Extended Data Fig. 3 | Summary of new and previously published isotopic data for the Rurutu-Arago hotspot track. Non-age-corrected plots of **A)**

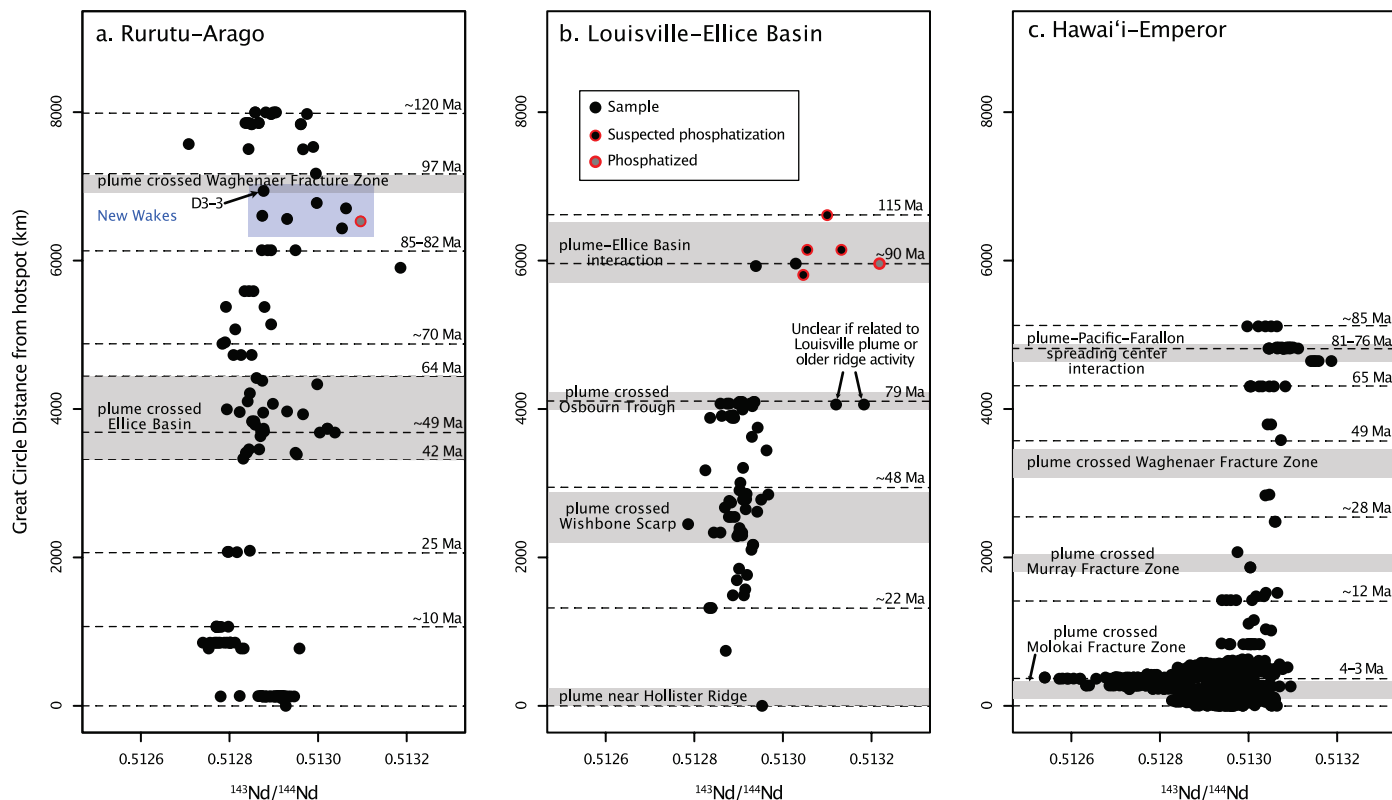
$^{207}\text{Pb}/^{204}\text{Pb}$ vs. $^{206}\text{Pb}/^{204}\text{Pb}$, **B)** $^{143}\text{Nd}/^{144}\text{Nd}$ vs. $^{206}\text{Pb}/^{204}\text{Pb}$, **C)** $^{208}\text{Pb}/^{204}\text{Pb}$ vs. $^{206}\text{Pb}/^{204}\text{Pb}$, **D)** $^{143}\text{Nd}/^{144}\text{Nd}$ vs. $^{87}\text{Sr}/^{86}\text{Sr}$, **E)** $^{143}\text{Nd}/^{144}\text{Nd}$ vs. $^{176}\text{Hf}/^{177}\text{Hf}$, **F)** $^{206}\text{Pb}/^{204}\text{Pb}$ vs. $^{87}\text{Sr}/^{86}\text{Sr}$, and **G)** $^{87}\text{Sr}/^{86}\text{Sr}$ vs. $^{176}\text{Hf}/^{177}\text{Hf}$ of our new Wake seamount samples (hexagons) compared to published data for the Tuvalu, Gilbert Ridge, Marshall/Ratak, and Wake Seamount portions of the Rurutu-Arago track (circles). Background data for young segments of the Cook-Austral plumes (Macdonald, Rurutu-Arago, Rarotonga), the Samoan plume, and Pacific MORB are given as 2σ contours of kernel density estimates (KDEs) of their respective datasets. Rarotonga lacks enough overlapping Sr, Pb, and Hf isotope data to be shown in panels **E** and **G**. Jurassic Pacific MORB data with seawater U alteration⁹² is also shown as small black open circles as a reference for how Pb isotopes may be disrupted in old seafloor basalts – and which is not evident in our new Wake samples (panels **A-D**). In both plots, the new Wake data plots within the known compositional range for the Wake Seamounts and the greater extent of the

track. One of the new samples (outlined in cyan in panels **A-C, F**) has unusually high $^{208}\text{Pb}/^{204}\text{Pb}$; this is a signature occasionally expressed in older Rurutu-Arago lavas and persists after strong leaching¹⁴. Here, $^{208}\text{Pb}/^{204}\text{Pb}$ is positively correlated with Th/U (see Extended Data Fig. 10), indicating U loss during alteration. Data are not corrected for post-eruptive radiogenic ingrowth (see Methods). We also identify a clear phosphatization signature (high Y/Y*; see Supplementary Data Table 1) in another of the new Wake samples (outlined in red in panels **B, D**, and **G**). As discussed in detail in the Supplement, strongly leached samples that have undergone significant phosphatization tend to have highly radiogenic $^{143}\text{Nd}/^{144}\text{Nd}$ of unclear origin. In such samples, Nd isotopes decouple from Sr isotopes (panel **D**) and Hf isotopes (panel **E**); obscuring some source mantle information. Here, $^{87}\text{Sr}/^{86}\text{Sr}$ vs. $^{176}\text{Hf}/^{177}\text{Hf}$ provide a more useful “isotopic fingerprint” of the HIMU-to-FOZO provenance characteristic of other Rurutu-Arago seamounts than plots using $^{143}\text{Nd}/^{144}\text{Nd}$, and are consistent with interpretations from the Pb isotopes.



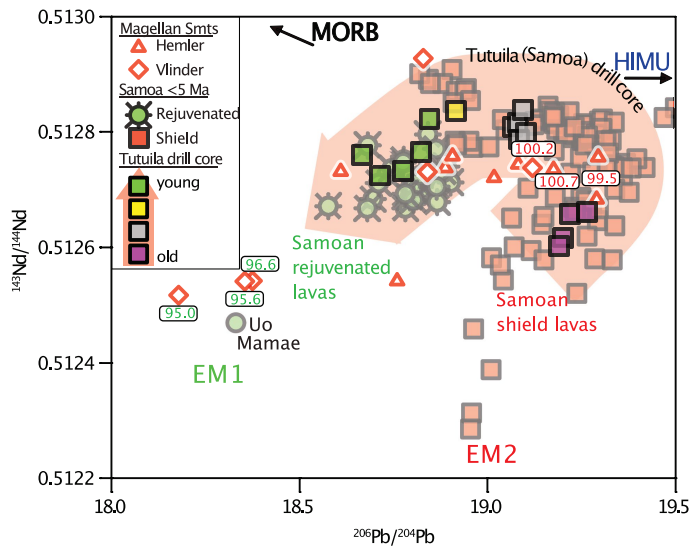
Extended Data Fig. 4 | Age-distance relationships of the Rurutu-Arago, Samoan, and Louisville plumes. A) Rurutu-Arago hotspot track. **B)** Samoa hotspot track. **C)** Louisville hotspot track. See Background Data Sources For Figures in Methods for data sources. Data shown here are only samples with age determinations or published age estimates (where well constrained by nearby volcanoes^{14,29} and Sr-Pb-Nd data to permit color coding. APM models are also included for reference (WK08⁴¹ = Wessel and Kroenke, 2008; D12⁶ = Doubrovine et al., 2012 without plume drift correction; K01¹⁸ = Koppers et al., 2001; K01m = modified Koppers et al., 2001 from this study). The oldest portions of the Hotspot Highway are in good agreement with K01m model predictions; some scatter occurs as a function of plume drift (e.g., Cretaceous portion of the Samoa hotspot; see Extended Data Fig. 8). For the hotspots shown here,

the data are consistent with age progressions that can be traced back into the Cretaceous, including the successful 91.3 Ma age determination from our new sample set. Rurutu-Arago has HIMU to FOZO-like compositions, while Samoan volcanoes are EM-type to FOZO in composition. The Rurutu-Arago age progression can be clearly traced into the Wakes and back to -120 Ma. The Samoan plume was active during the Cretaceous, forming the Magellan chain in the West Pacific where EM2 and EM1 compositions consistent with those found in Samoan shield and rejuvenated volcanoes, respectively (see Extended Data Fig. 6 for details). The FOZO Louisville hotspot track and older Ellice Basin Seamounts as well as Seka Seamount; which are likely FOZO-to-DMMlike with Pb isotopes partly overprinted by seawater U ingrowth, are also age-progressive.

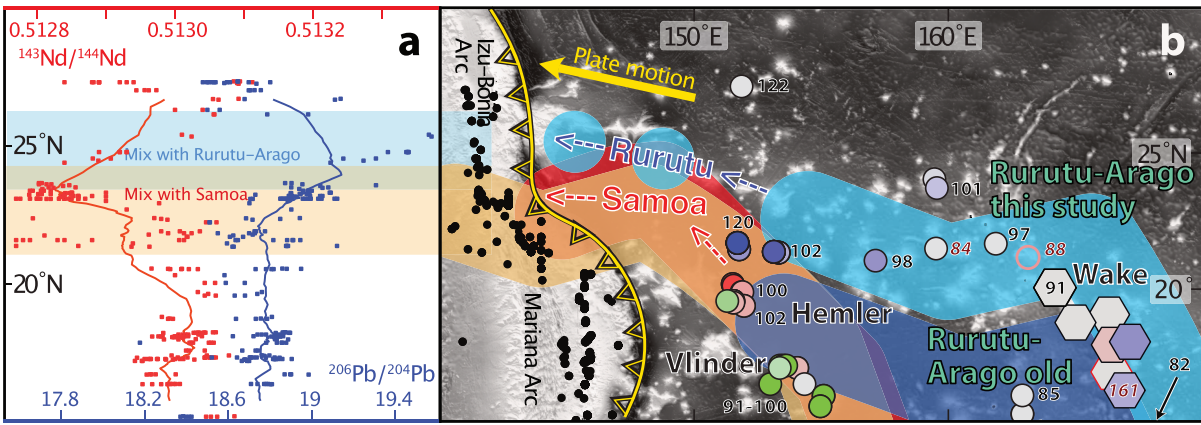


Extended Data Fig. 5 | Great circle distance (km) from active hotspot center vs. $^{143}\text{Nd}/^{144}\text{Nd}$ (not age-corrected) for hotspot tracks with and without plume-ridge interaction. A) Rurutu-Arago, B) Louisville-Ellice Basin Seamounts, and C) Hawai'i-Emperor hotspot tracks. Isochrons are provided as dashed lines, and light grey fields mark where the plumes interacted with ridges or fracture zones. All three hotspot tracks record significant variability in isotopic composition over time that correspond to interaction of the plume with major lithospheric structural features. Rurutu-Arago, which was a true-intraplate hotspot for the entirety of its documented history, produced episodes of depleted (high $^{143}\text{Nd}/^{144}\text{Nd}$) melts that coincide spatially with major lithospheric structures, but otherwise maintains a fairly constant $^{143}\text{Nd}/^{144}\text{Nd}$ over time. Samples with evidence of phosphatization (high Y/Y^* and/or P_2O_5 ; see Extended

Data Fig. 10) are shown as light grey circles with red outlines. Black circles with red outlines are samples that may have been phosphatized ($^{143}\text{Nd}/^{144}\text{Nd} > -0.5131$) but cannot be confirmed due to lack of available major and trace element data. By contrast, the Louisville hotspot track, including the Ellice Basin Seamounts, records a long-term trend of enrichment with time that records its transition from plume-ridge interaction to true intraplate. Deviations also occur when the plume crossed the Osborn Trough (however, it remains unclear whether this is related to the Louisville plume), and later the Wishbone Scarp (attributed to source mantle heterogeneity^{29,64}). The broad enrichment trend in Louisville is similar to long-term enrichment observed in the Hawaiian plume, which also interacted with a ridge in the Cretaceous before transitioning to a true-intraplate plume system¹¹². Data sources are the same as in Fig. 1.

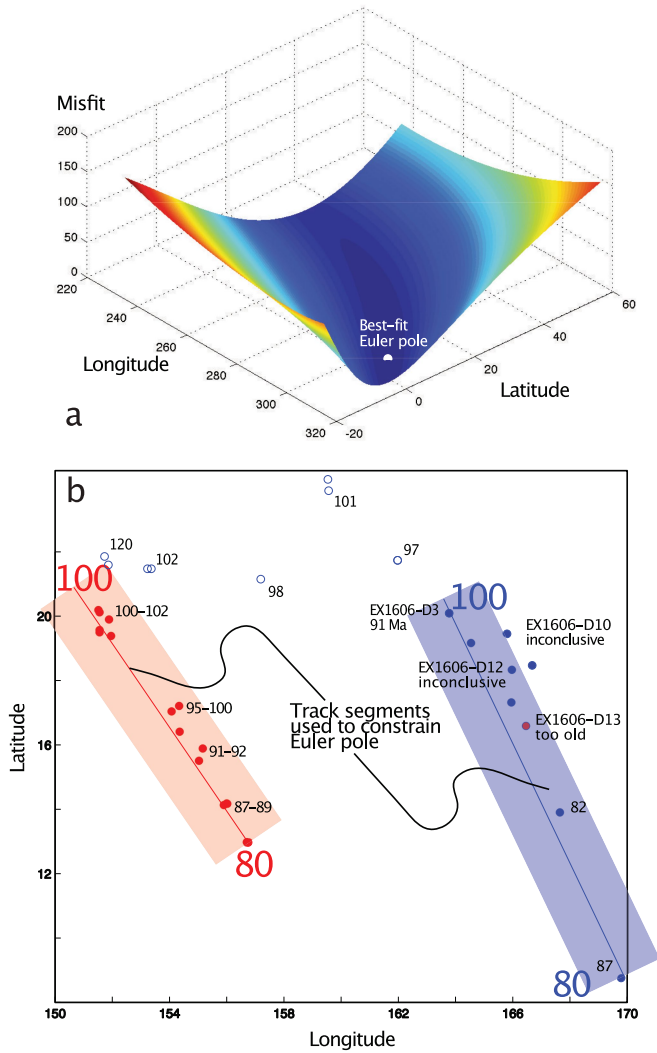


Extended Data Fig. 6 | Compositional overlap between modern Samoa (<5 Ma) and Cretaceous Samoan volcanoes—Hemler and Vlinder seamounts—in the West Pacific. Most of the geochemical evolution of Samoan volcanoes through time is reflected in a drill core into Tutuila Island (Samoa⁴⁹). This shows (red arrow) a change in lava compositions from shield to rejuvenated lavas, with volcanoes active over the past 5 Ma¹⁴. The older samples^{31,91} (ages shown in white text bubbles) from Hemler and Vlinder (-100 Ma) mainly plot around the shield lavas in Samoa while the youngest samples (-95 Ma) continue through the rejuvenated lavas represented by the most extreme EM1 type composition in the Samoan area (Uo Mamae¹⁹).



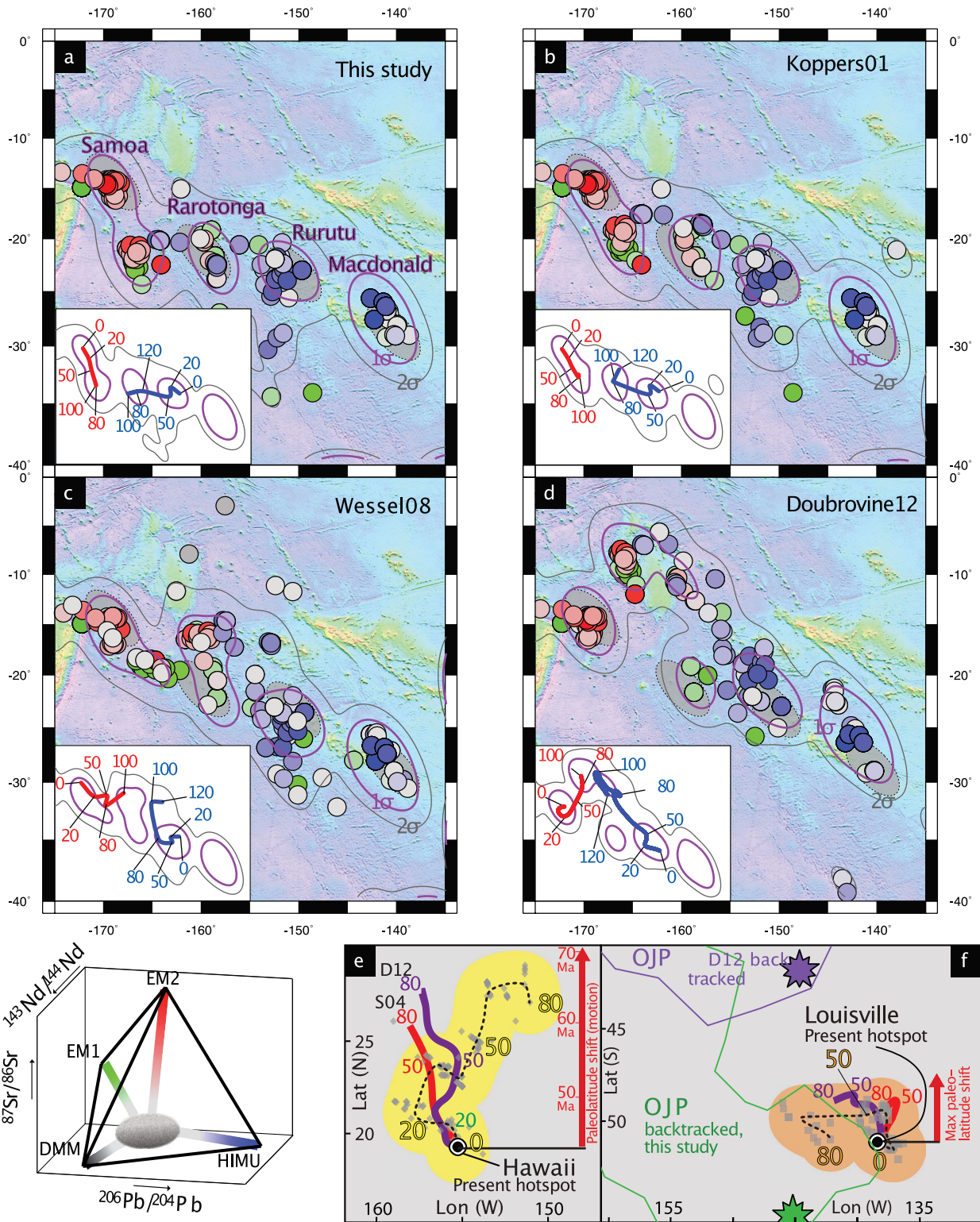
Extended Data Fig. 7 | Map of West Pacific seamounts, showing Rurutu-Arago and Samoa predicted hotspot tracks (K01¹⁸ in dark shade, this study in light shade). A) $^{143}\text{Nd}/^{144}\text{Nd}$ (red) and $^{206}\text{Pb}/^{204}\text{Pb}$ (blue) compositions of Izu-Bonin-Mariana arc volcanoes⁵² versus latitude. **B)** Corresponding map of the West Pacific with model reconstructions illustrating predicted locations where the Rurutu-Arago and Samoa hotspot tracks are subducted. Black numbers with white outline represent ages^{31,115}, while numbers in red represent likely unrelated volcanic ages, given large age difference with expected age along the hotspot track and difference in composition (pink circle³¹). New Wake region isotope data (hexagons) and a 91.3 Ma age determination provides the “missing link” that suggests that Rurutu hotspot continues through the

seamounts west of Wake Island. The samples outlined with red has $^{143}\text{Nd}/^{144}\text{Nd}$ affected by phosphatization. The existing (dark blue¹⁸) APM model track for the Rurutu-Arago hotspot is devoid of major seamounts, while the new track (light blue) continues the unusual isotopic composition and morphological chain to the Izu-Bonin-Mariana trench. A similar prediction for Samoa (red: K01¹⁸; orange: updated) shows both hotspots have a corresponding unusual spike in isotopic compositions in the arc (left panel; lines represent running means), indicating prior subduction of a continuing chain of similar composition, mixing Rurutu-Arago (HIMU) or Samoa (EM2) hotspot material into the mantle wedge.



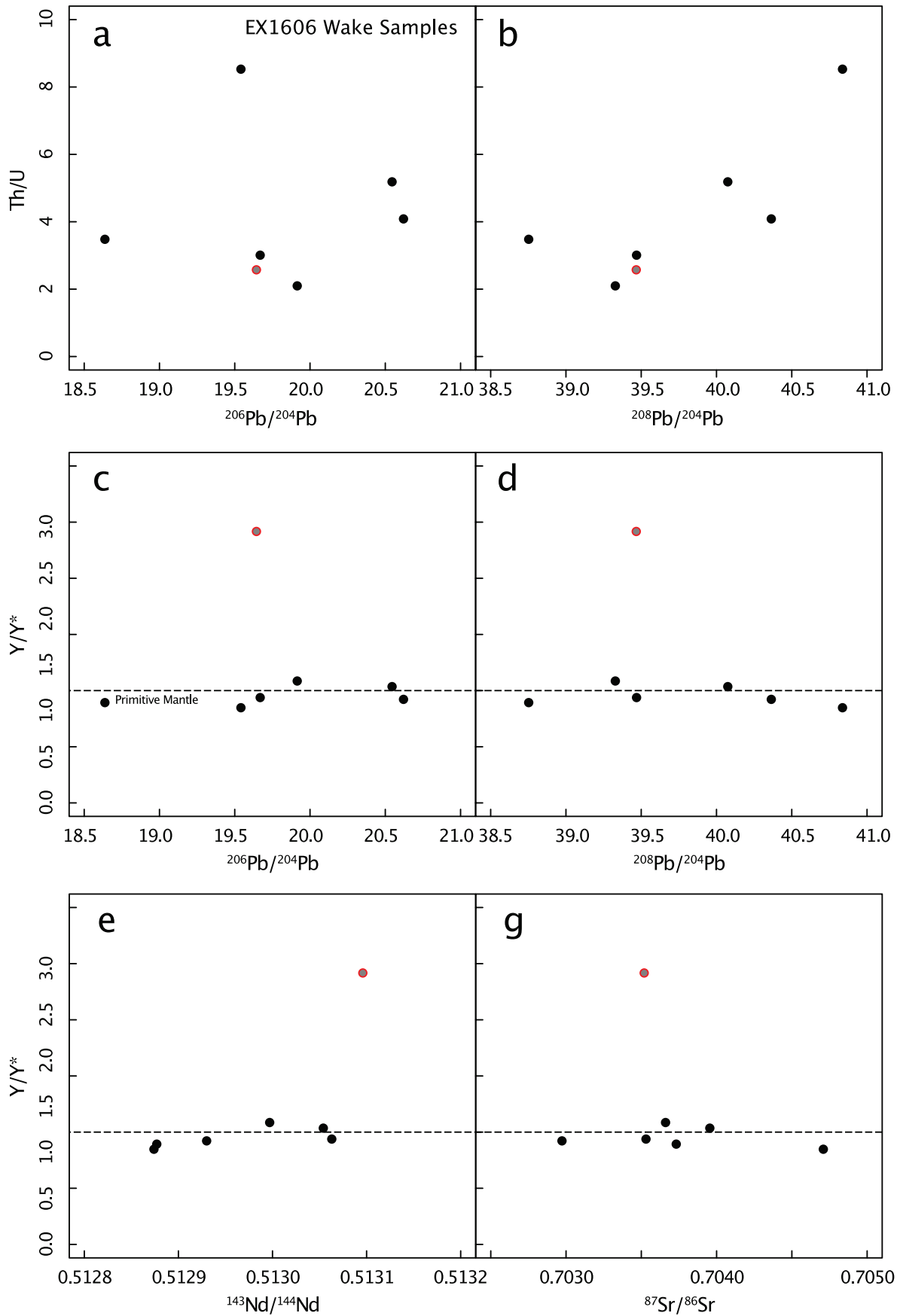
Extended Data Fig. 8 | Determination of the updated 100-80 Ma Euler Pole.

A) Rotation (Euler) pole modeling is accomplished by a grid search for the best-fit pole (0.7°S , 315.7°E), shown as the latitude-longitude location for which the minimum misfit is found (white dot). **B)** Constraints for the modeled rotation are the colored seamount locations (blue and red, selected based on their apparent fit in composition), and the approximate age range for these volcanic tracks (80–100 Ma), based on model-specific, new, and adjacent seamount volcanic ages^{31,91} (black numbers next to seamount markers). Only two samples from EX1606 had material suitable for age dating, but four of the samples were attempted. Two succeeded, with one yielding a 91.3 Ma age that confirms that the Rurutu-Arago plume was active in the Wake region. The second successful sample predates passage of this area of the Pacific crust over the Rurutu-Arago hotspot and is excluded as a constraint on the modified stage pole. The two unsuccessful samples lacked a statistically robust plateau and were therefore inconclusive. Open circles represent Wake area seamounts and their ages, predating the 80–100 Ma time period modeled.



Extended Data Fig. 9 | Backtracked original eruptive locations for Samoa and Cook-Austral-related volcanoes (Cook-Austral, Samoa, Tuvalu, Gilbert, Wake, Magellan, Tokelau), using various absolute plate motion models. A) this study; B) Koppers01¹⁸; C) Wessel08⁴¹; D) Doubrovine12⁶. Backtracked seamounts color-coded (lower left panel) for their isotopic compositions show that at present-day hotspots (purple text) are the focus of clusters of consistent geochemical compositions, defined by grey (2) and purple (1) contours for Gaussian-kernel probability density estimates for the backtracked locations. Insets show these density contours and the running mean of backtracked location and age to estimate plume motion from model

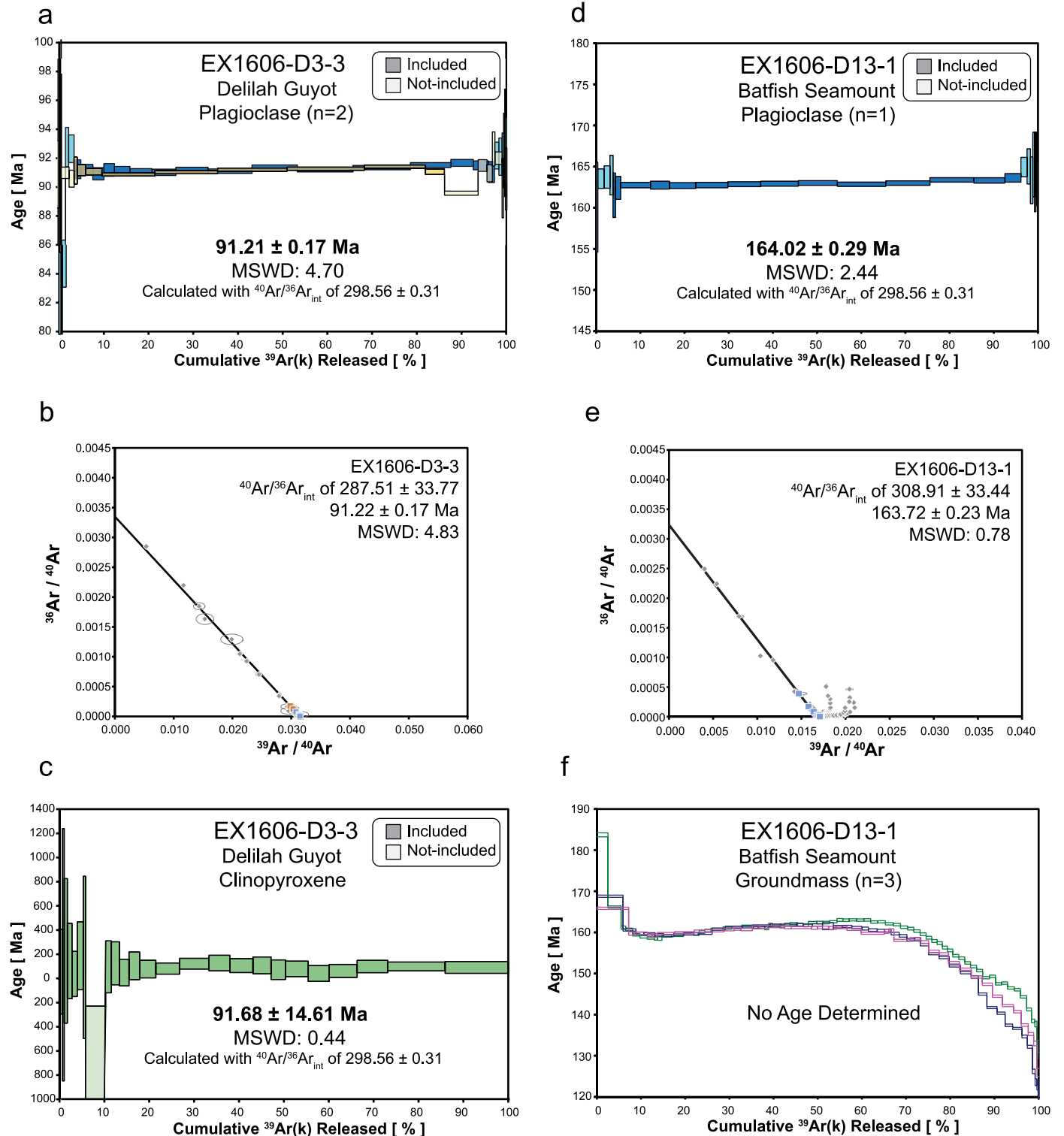
mismatch from fixed hotspots (a-d). Backtracked (grey symbols⁶) locations for Hawai'i (E) and Louisville (F) and their smoothed age-track (wide yellow or orange) highlight a deviation from predicted plume motion (S04/red¹⁰⁰ and D12/purple⁶) beyond 50 Ma, indicating a mismatch for plate motion models into the Cretaceous. Outlines show Ontong-Java Plateau (OJP) backtracked with the new model overlap with Louisville, where stars show approximate center of Ontong-Manihiki-Hikurangi. Red arrows show smoothed tracks match derived latitudinal plume motion from paleomagnetic latitudes^{13,96}. Backtracking of OJP assumes fixed relationship to the Pacific plate, with no rotation of the plateau¹¹.



Extended Data Fig. 10 | See next page for caption.

Extended Data Fig. 10 | Trace element alteration proxies versus Sr-Nd-Pb isotope compositions of the new Wakes (EX1606) samples. A) Th/U versus measured $^{206}\text{Pb}/^{204}\text{Pb}$, **B)** Th/U versus measured $^{208}\text{Pb}/^{204}\text{Pb}$, and **C-F)** Y/Y^* versus radiogenic isotope compositions. Versus Th/U, $^{206}\text{Pb}/^{204}\text{Pb}$ (**A**) exhibits only a weak correlation with Th/U, while $^{208}\text{Pb}/^{204}\text{Pb}$ (**B**) is much more strongly

correlated, indicating modification of U abundances in the EX1606 samples. $^{143}\text{Nd}/^{144}\text{Nd}$ (**E**) exhibits some correlation versus Y/Y^* , a proxy for phosphatization, becoming more radiogenic at high Y/Y^* , while Pb and Sr isotopes show no correlation.



Extended Data Fig. 11 | $^{40}\text{Ar}/^{39}\text{Ar}$ Age determinations for EX1606-D3-3 and EX1606-D13-1. **A)** Stacked EX1606-D3-3 age plateau from plagioclase separates for Batfish Seamount (n = 2). Included steps are shown in dark blue and dark yellow, and not included steps are shown in light blue and light yellow. **B)** Inverse Isochron for EX1606-D3-3 plagioclase separates (n = 2). Included steps are shown in blue and yellow, and not included steps are shown in grey. The solid line indicates the measured $^{40}\text{Ar}/^{36}\text{Ar}$ initial ratios. **C)** EX1606-D3-3 age plateau from a clinopyroxene separate. Included steps are shown in dark

green, and not-included steps are shown in light green. **D)** EX1606-D13-1 age plateau from plagioclase separates at Unnamed Seamount (n = 1). Included steps are shown in dark blue and not-included steps are shown in light blue. **E)** Inverse isochron for EX1606-D13-1 for groundmass and plagioclase separates (n = 4). Included steps are shown in blue, and not included steps are shown in grey. The solid line indicates the measured $^{40}\text{Ar}/^{36}\text{Ar}$ initial ratios **F)** Stacked EX1606-D13-1 age plateau determinations for groundmass separates. None of the groundmass experiments produced a concordant age determination.

Extended Data Table 1 | Stage poles for the Modified Pacific Hotspot Reference Frame Absolute Plate Motion Model (italics from KO1¹⁸)

Stage start (Ma)	Stage end (Ma)	Latitude (°N)	Longitude (°E)	Rotation Rate (°/Myr)	Standard Deviation
<i>0</i>	<i>20</i>	<i>70.1</i>	<i>302.0</i>	<i>0.88</i>	<i>0.016</i>
<i>20</i>	<i>43</i>	<i>67.1</i>	<i>294.5</i>	<i>0.58</i>	<i>Not given</i>
<i>43</i>	<i>80</i>	<i>18.8</i>	<i>253.6</i>	<i>0.66</i>	<i>0.029</i>
<i>80</i>	<i>100</i>	<i>-0.7</i>	<i>315.7</i>	<i>0.975</i>	<i>0.06</i>
<i>100</i>	<i>110</i>	<i>75.1</i>	<i>44.8</i>	<i>0.44</i>	<i>Not given</i>
<i>110</i>	<i>125</i>	<i>65.3</i>	<i>273.2</i>	<i>0.45</i>	<i>0.042</i>

	Latitude (°N)	Longitude (°E)
Magellan Seamounts:		
1	20.17	151.53
2	19.48	151.57
3	19.55	151.57
4	20.1	151.57
5	19.88	151.9
6	19.37	151.97
7	17.03	154.07
8	17.2	154.33
9	16.4	154.35
10	15.5	155.02
11	15.88	155.15
12	14.13	155.88
13	14.18	155.98
14	14.17	156
15	12.98	156.68
16	12.97	156.75
Marshall Seamounts:		
17	20.45	163.72
18	19.15	164.56
19	19.45	165.8
20	17.31	165.96
21	18.32	165.98
22	18.47	166.68
23	13.9	167.65
24	8.76	169.79